NAVAL POSTGRADUATE SCHOOL

MONTEREY, CALIFORNIA

THESIS

A NEW TECHNIQUE FOR ROBOT VISION IN AUTONOMOUS UNDERWATER VEHICLES USING THE COLOR SHIFT IN UNDERWATER IMAGING

by

Jake A. Jones

June 2017

Thesis Advisor: Roberto Cristi
Co-Advisor: Xiaoping Yun

Approved for public release. Distribution is unlimited.

THIS PAGE INTENTIONALLY LEFT BLANK

REPORT DOCUMENTATION PAGE			*Form Approved OMB No. 0704-0188*
Public reporting burden for this collection of information is estimated to average 1 hour per response, including the time for reviewing instruction, searching existing data sources, gathering and maintaining the data needed, and completing and reviewing the collection of information. Send comments regarding this burden estimate or any other aspect of this collection of information, including suggestions for reducing this burden, to Washington headquarters Services, Directorate for Information Operations and Reports, 1215 Jefferson Davis Highway, Suite 1204, Arlington, VA 22202-4302, and to the Office of Management and Budget, Paperwork Reduction Project (0704-0188) Washington, DC 20503.			
1. AGENCY USE ONLY ***(Leave blank)***	**2. REPORT DATE** June 2017	**3. REPORT TYPE AND DATES COVERED** Master's thesis	
4. TITLE AND SUBTITLE A NEW TECHNIQUE FOR ROBOT VISION IN AUTONOMOUS UNDERWATER VEHICLES USING THE COLOR SHIFT IN UNDERWATER IMAGING			**5. FUNDING NUMBERS**
6. AUTHOR(S) Jake A. Jones			
7. PERFORMING ORGANIZATION NAME(S) AND ADDRESS(ES) Naval Postgraduate School Monterey, CA 93943-5000			**8. PERFORMING ORGANIZATION REPORT NUMBER**
9. SPONSORING /MONITORING AGENCY NAME(S) AND ADDRESS(ES) N/A			**10. SPONSORING / MONITORING AGENCY REPORT NUMBER**
11. SUPPLEMENTARY NOTES The views expressed in this thesis are those of the author and do not reflect the official policy or position of the Department of Defense or the U.S. Government. IRB number ____N/A____.			
12a. DISTRIBUTION / AVAILABILITY STATEMENT Approved for public release. Distribution is unlimited.			**12b. DISTRIBUTION CODE**

13. ABSTRACT (maximum 200 words)

Developing a technique for underwater robot vision is a key factor in establishing autonomy in underwater vehicles. A new technique is developed and demonstrated to depict an underwater scene in three dimensions (3D) for use in underwater robot vision. This technique uses passive lighting and the optical properties of water to approximate distances between objects in a scene.

Beer's Law is used to describe the change in intensity that light at different wavelengths experiences as it travels through water. If the intensities can be measured, then Beer's Law provides sufficient information to estimate the unknown distance. Applying the equation pixel by pixel to compare two images produces distances from the camera to everything in the image. A shift in color caused by the uneven absorption by each wavelength is similar to comparing the intensities. The color shift produces a relative distance between objects in the scene rather than distances from the camera to the objects. This relative distance may be combined with other techniques to determine the distances from each pixel to the camera.

14. SUBJECT TERMS unmanned undersea vehicles (UUVs), autonomous underwater vehicles (AUVs), robot vision, autonomy, visual odometry, underwater color shift, optical properties of water			**15. NUMBER OF PAGES** 75
			16. PRICE CODE
17. SECURITY CLASSIFICATION OF REPORT Unclassified	**18. SECURITY CLASSIFICATION OF THIS PAGE** Unclassified	**19. SECURITY CLASSIFICATION OF ABSTRACT** Unclassified	**20. LIMITATION OF ABSTRACT** UU

NSN 7540-01-280-5500 Standard Form 298 (Rev. 2-89) Prescribed by ANSI Std. 239-18

THIS PAGE INTENTIONALLY LEFT BLANK

Approved for public release. Distribution is unlimited.

A NEW TECHNIQUE FOR ROBOT VISION IN AUTONOMOUS UNDERWATER VEHICLES USING THE COLOR SHIFT IN UNDERWATER IMAGING

Jake A. Jones
Lieutenant Commander, United States Navy
B.S., Brigham Young University, 2003
M.S., Oregon State University, 2011

Submitted in partial fulfillment of the
requirements for the degree of

MASTER OF SCIENCE IN ELECTRICAL ENGINEERING

from the

NAVAL POSTGRADUATE SCHOOL
June 2017

Approved by: Roberto Cristi
Thesis Advisor

Xiaoping Yun
Co-Advisor

R. Clark Robertson
Chair, Department of Electrical and Computer Engineering

THIS PAGE INTENTIONALLY LEFT BLANK

ABSTRACT

Developing a technique for underwater robot vision is a key factor in establishing autonomy in underwater vehicles. A new technique is developed and demonstrated to depict an underwater scene in three dimensions (3D) for use in underwater robot vision. This technique uses passive lighting and the optical properties of water to approximate distances between objects in a scene.

Beer's Law is used to describe the change in intensity that light at different wavelengths experiences as it travels through water. If the intensities can be measured, then Beer's Law provides sufficient information to estimate the unknown distance. Applying the equation pixel by pixel to compare two images produces distances from the camera to everything in the image. A shift in color caused by the uneven absorption by each wavelength is similar to comparing the intensities. The color shift produces a relative distance between objects in the scene rather than distances from the camera to the objects. This relative distance may be combined with other techniques to determine the distances from each pixel to the camera.

THIS PAGE INTENTIONALLY LEFT BLANK

TABLE OF CONTENTS

THIS PAGE INTENTIONALLY LEFT BLANK

LIST OF FIGURES

LIST OF TABLES

THIS PAGE INTENTIONALLY LEFT BLANK

LIST OF ACRONYMS AND ABBREVIATIONS

3D	Three Dimensions
AUV	Autonomous Underwater Vehicle
HD	High Definition
MIT	Massachusetts Institute of Technology
ONR	Office of Naval Research
RGB	Red Green Blue
ROVs	Remote Operated Vehicles
UUVs	Unmanned Undersea Vehicles

THIS PAGE INTENTIONALLY LEFT BLANK

ACKNOWLEDGMENTS

I would like to acknowledge the help and support from my parents. My beautiful wife and my kids have been supportive and have served as my inspiration to keep pushing forward. My family is my life and I couldn't have done this without them. Thank you, sweetheart, for letting me travel and dive and spend money out of our pockets to make sure this research happened. I would also like to thank Tom Diehl for volunteering to be my dive buddy to collect my data; without his sacrifice I couldn't have completed this project. My cousin Megan Jones was also instrumental in proofreading and editing my paper. I would also like to thank James Calusdian for his help and support in the lab. He has always been available when I need to exchange ideas. Finally, I would like to thank my advisors. I am especially grateful to Dr. Roberto Cristi for taking me on last minute so I didn't have to start all over again, and I appreciate Dr. Yun and his dedication to education.

THIS PAGE INTENTIONALLY LEFT BLANK

I. INTRODUCTION

Unmanned vehicles have emerged as the next wave of technology to populate the battlefield. Whether this technology will dominate the battlespace is still uncertain, but one thing is certain: unmanned vehicles have already changed how we operate. Unmanned systems have allowed access to previously inaccessible areas, increased mission efficiency, and extended the reach of a host platform. They provide valuable time-sensitive information. The U.S. Navy defines unmanned undersea vehicles (UUVs) as "self-propelled submersibles whose operation is either fully autonomous or under minimal supervisory control and is untethered except, possibly, for data links such as a fiber optic cable" [1]. This definition is not meant to encompass Remote Operated Vehicles (ROVs) [1].

During Operation Iraqi Freedom, UUVs were used to clear mines in the Persian Gulf [1]. Other UUVs have been used to conduct oceanographic surveys or underwater inspections. The Navy is focusing on nine missions according to the UUV master plan: "Intelligence, Surveillance, and Reconnaissance; Mine Countermeasures; Anti-Submarine Warfare; Inspection / Identification; Oceanography; Communication / Navigation Network Nodes; Payload Delivery; Information Operations; and Time Critical Strike" [1]. The UUV master plan also states that unmanned vehicles will serve as force multipliers and risk reduction agents in these missions. The long-term UUV vision is "to have the capability to: (1) deploy or retrieve devices; (2) gather, transmit, or act on all types of information; and (3) engage bottom, volume, surface, air, or land targets" [1].

UUVs must be autonomous, deployable, adaptable, persistent, and low profile to contribute to the needs of the Navy in accomplishing the intended missions. As set forth in the UUV master plan [1], autonomy is the ability to operate independently for extended periods of time. It also describes deployable as meaning that the UUV can be easily deployed and recovered from a variety of platforms and in large quantities. Persistence refers to a vehicle's ability to stay on station for long periods of time, including in adverse weather conditions as described by the UUV master plan. Low

profile means that the vehicle will operate covertly with low acoustic and electromagnetic signature [1]. Autonomy is considered the largest long-term challenge for UUVs, followed closely by the power and energy technology, according to a study performed by the RAND Corporation [2].

The Office of Naval Research (ONR) has defined six levels of vehicle autonomy:

1) Fully Autonomous defines a system that "requires no human intervention to perform any of its designed activities" [3].

2) Mixed Initiative describes an autonomous system that allows either the system or a human to react to sensed data. "The system can coordinate its behavior with human behavior both explicitly and implicitly" [3].

3) A Human Supervised system "can perform a wide variety of activities once given top-level permission or direction by a human" [3].

4) Human Delegated systems "can perform limited control activities on a delegated basis" [3].

5) Human Assisted systems "can perform activities in parallel with human input… However, the system has no ability to act without accompanying human input" [3].

6) Human Operated defines a system with no autonomy [3].

For the purpose of this research, Autonomous Underwater Vehicles (AUVs) will include vehicles described by the third and fourth categories, and Remotely Operated Vehicles (ROVs) will include vehicles from the fifth and sixth categories. There are not currently any underwater vehicles that would be classified in the first two categories.

ROVs require a full-time remote operator, a tether for power and data transfer, and a camera for the operator to see the environment. AUVs are generally programmed to swim a specific path and do not require an operator or a tether. Tethered vehicles restrict the host platform, create entanglement scenarios, may be difficult to recover quickly and are, therefore, not suitable for the battlefield except in very specific circumstances [1]. A tether is helpful during research and development as UUVs progress to fulfill the intended missions. Current technology and design are not yet sufficient for autonomous vehicles to accomplish most of the specified missions [4].

Increased autonomy is required to conduct the desired missions [1]. To achieve the required level of autonomy, vehicles must be able to sense, process, and react to both static and dynamic environments. Robot vision is defined as the combination of hardware and software algorithms to allow a robot to process its environment [5]. Robot vision must be developed first to sense and process the environment before controllers can be developed to employ these techniques.

Sensors currently available include various sonar systems, laser rangefinders, structured light, and visual odometry. Of these many sensors, none are ready for development into controllers for an AUV to rapidly adapt to a changing environment [2]; although, there is a lot of research currently underway to move in that direction. With current technology, either sensing the environment takes too long or processing the data is beyond the onboard capability; therefore, developing a successful form of robot vision for AUVs is a worthwhile field of study.

A. RESEARCH OBJECTIVE

The purpose of this research is to demonstrate a new technique for underwater robot vision using image analysis that may be developed into a controller for AUVs. Analyzing the change in wavelength-specific light intensity as it travels through water from an object to a camera may be used to approximate the distance between the object and the camera. If the intensities cannot be measured, then a relative distance can be determined by comparing the color shift that light experiences between the object and the camera. This technique uses a camera, a filter, and relies on the existence of natural light.

B. THESIS LAYOUT

This thesis begins with a description of robot vision and a brief discussion of advantages or obstacles for adapting these sensors in Chapter II. The development of a new technique for underwater robot vision using a color shift is described in Chapter III. The equipment and design used to collect and analyze data to prove the technique is included in Chapter IV. The results are summarized, including conclusions and recommendations for future work, in Chapter V.

THIS PAGE INTENTIONALLY LEFT BLANK

II. BACKGROUND

A. ROBOT VISION

Current sensors are insufficient to develop into useful underwater robot vision. The time required to gather and process the data takes too long. Three knots is considered a low speed for an AUV. At this speed the AUV is moving 1.54 meters per second (5.05 feet per second). The environment needs to be sensed, interpreted, and a course correction made within a fraction of this time to avoid obstacles.

Most AUVs are programmed to swim a specific pattern and area without being able to "see" where it is going at all. The AUV will use onboard sensors such as an echo sounder, Global Positioning System, Inertial Measurement Unit, or Doppler Velocity Log to verify its position and continue along its preprogrammed path. If there happens to be a new object in its path or if it deviates from its programmed course it can get lost or stuck.

There are currently many sensors and techniques under development for underwater robot vision. There are laser-based sensors, which project a laser and calculate ranges based on time-of-flight calculations while making some assumptions about the scene geometry [6]. One method developed by Cain and Leonessa [6] and further work by Hansen et al. [7] utilizes two line lasers and a camera to provide a two-dimensional and three-dimensional representation of the environment, respectively. Several other laser-based systems have been developed by researchers such as Karras and Kyriakopoulos [8], Jaffe [9], and Campos and Codina [10]. The approach by Campos and Codina bridges the next subject in that it uses lasers to project structured light patterns to determine the shape of objects in the environment.

Structured light is a technique that has recently received some attention. Structured light works like laser scanners by projecting light and then viewing the reflected light with a camera set at an angle. The difference is that the light projected has a specific pattern instead of just a point or beam. Comparing the expected pattern (assuming no object in the path of the light) to the actual return can determine the shape of the object that caused the distortion. The projected light may be black and white,

colored or even at higher frequencies such as infrared or ultraviolet and may be projected in an infinite variety of patterns [10]–[14]. Other variations may include two or more cameras at various angles to improve accuracy or to compensate for the directionality of the pattern [15]–[17]. Different patterns may be projected sequentially and then stitched together to form a point cloud. The resolution of the resultant point cloud is limited by the resolution and complexity of the projected pattern.

Another method of robot vision is based on a technique called visual odometry. "Visual odometry is the process of determining the position and orientation of a robot by analyzing associated camera images" [18]. Images are acquired using either a single camera or multiple cameras working in stereo or omnidirectional cameras [19]–[24]. Visual odometry can be done at a fraction of the cost and computing power of other robot vision methods [19]. It has been studied for decades and may be the answer to autonomy in underwater vehicles.

B. THE BEER–LAMBERT LAW

The way light interacts with the ocean is peculiar and has been studied for decades. Light changes as it enters the water and as it travels to the depths it continues to change. Perception of light underwater changes as well. Because of refraction, objects appear larger underwater unless viewed through a domed lens. Colors are difficult to see. Most things appear as a shade of green and the deeper one goes the darker and colder everything appears.

Most light that reaches the ocean surface is transmitted into the sea and attenuated in the water below. Attenuation is due to absorption and scattering as discussed by Kirk [25]. Absorption is of particular interest because light at different wavelengths experiences higher or lower absorption over the same distance. Red light is absorbed over a short distance and may only travel up to 10 m through clear salt water, whereas green light may travel up to 25 times as far before it is absorbed, as seen in Figure 1 [26]. Light travels significantly less distance in coastal waters as seen in the right-hand side of Figure 1. This is primarily due to scattering. More particulate in the water causes the light to scatter before it can be absorbed. Some regions have such high concentrations of

particulate that none of the wavelengths travel more than a few inches; in other words, nothing is visible even inches away.

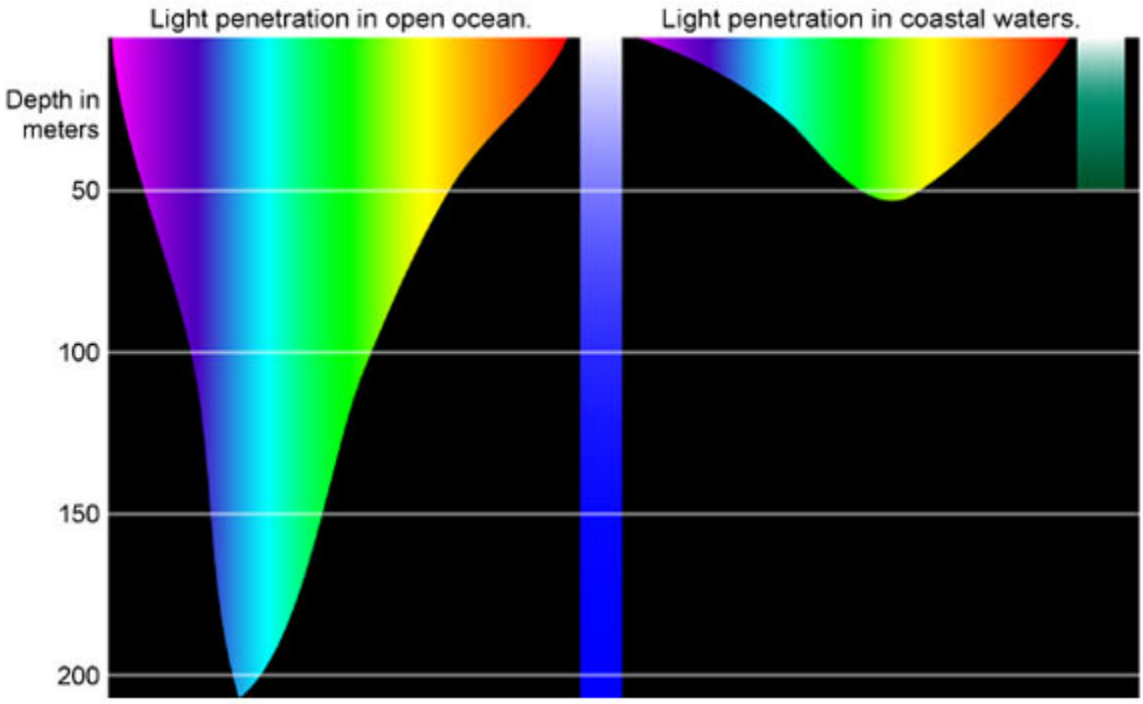

Figure 1. Patterns of Light Penetration in Open Water and Coastal Water. Source: [27].

Underwater photography and videography requires additional light sources or filters to restore visible wavelengths of light to compensate for this absorption [28]. This absorption is predictable and is used to develop robot vision. The absorption of light in water may be described by the Beer–Lambert law [29],

$$I_d = I_0 e^{-\alpha d}, \tag{2.1}$$

where I_d represents the intensity of the light at a given distance d and I_0 represents the intensity of the light at the source. The absorption coefficient is represented by α. It is easy to see that this represents an exponential decay proportional to the distance and absorption coefficient for a given wavelength. Many studies have been done to determine the specific absorption coefficients at various wavelengths in pure water as well as other

fluids to improve our understanding of the relationship between light and water [30]–[32].

C. COLOR SPACE

RGB values are related to three standard primaries called X, Y, and Z by the International Commission on Illumination or Commission Internationale de l'Éclairage (CIE) as early as 1931 [33], [34]. The XYZ color space is an international standard used to define colors that is invariant across devices and is seen in Figure 2. These primaries are then correlated to specific wavelengths of light. This comparison links the physical pure colors to the physiological perceived colors and defines the XYZ color space and the RGB color space [34], [35]. The RGB color space varies between devices as a local device's interpretation of the XYZ color space standard. The Adobe RGB primary triangle is also shown in Figure 2. It is noted that colors outside this triangle cannot be represented when adopting the Adobe RGB standard. The Adobe RGB color space is only able to represent about 50 percent of the XYZ color space but is the best representation currently available.

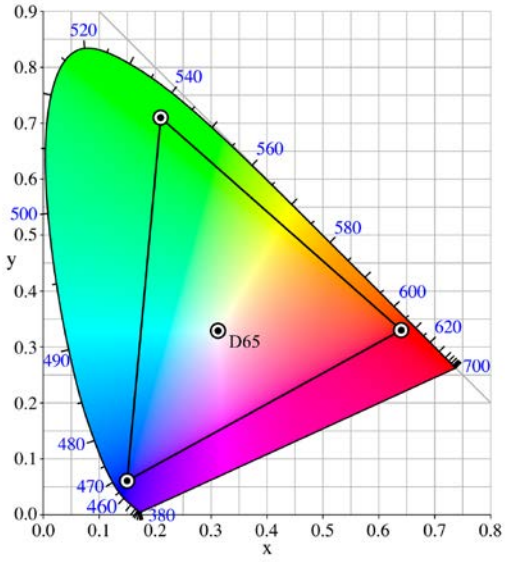

Figure 2. CIE XYZ Color Space Including Adobe RGB Triangle and D65 White Standard. Source: [36].

The (x,y) values in the triangle in Figure 2 are correlated with corresponding RGB values between zero and one. Corners correspond to the points in Table 1 [36]. Each red, green, and blue value that makeup a color is typically stored as an 8-bit byte for most devices, although higher resolution is available on some devices. A one corresponds to 255, and each corner is represented as (255,0,0) "red," (0,255,0) "green," and (0,0,255) "blue." For every fraction of each of these values there is a corresponding wavelength of color. For example, a wavelength of 620 nm corresponds to an RGB value of (255,0,0) or (1,0,0), the brightest red. "Brightest" may be misleading and refers to the shade of red and not the typical brightness. The combination of RGB values indicates the color of a pixel but is independent of intensity.

Table 1. Red, Green, Blue Primaries in Adobe RGB Color Space Correlated to (x,y) Values. Adapted from [36].

	x	y	R	G	B
Red	0.64	0.33	1	0	0
Green	0.21	0.71	0	1	0
Blue	0.15	0.06	0	0	1
White	0.3127	0.329	1	1	1

D. LUMINOUS INTENSITY

The intensities described in Equation (2.1) are luminous intensities and are measured in candela or lumen per steradian. Luminous intensity is the wavelength-weighted quantity of visible light that is emitted per unit time per solid angle [37]. By definition, "if a light source emits monochromatic green light with a wavelength of 555 nm and has a radiant intensity of 1/683 watts per steradian in a given direction, that light source will emit one candela in the specified direction" [38]. A submersible radiometer has been designed by Morrow et al. [39] to "measure ultraviolet and visible light and detect extremely low light levels in the deep sea. They numerically describe the shape of

the light field in the ocean and measure how light is absorbed and scattered in water over small spatial scales" [39]. These radiometers may be used to precisely measure the intensity of various wavelengths or, more importantly, the change in the intensity of a specific wavelength over a given distance.

E. CORRECTING FOR TEMPERATURE AND SALINITY

Pinpointing the specific absorption coefficient proves difficult as it varies with temperature, salinity, and turbidity. It may vary for the same location because of seasonal changes in temperature and salinity and even over short periods of time based on a local event. Even in a spot in the middle of the ocean where the temperature and salinity have little seasonal variation and the water is very clear, there are thermal layers and pockets that do not mix well throw off this calculation. The chosen wavelength of light to use can improve this estimate; likewise comparing between several wavelengths may also mitigate these inaccuracies.

The absorption coefficient can be corrected for temperature and salinity [40]. These coefficients have been spectrophotometrically measured and verified using a point-source integrating cavity absorption meter [41]. Shorter wavelengths have a positive correlation with temperature, and longer wavelengths have a negative correlation with temperature centered around 650 nm [41]. These corrections are made by adding the temperature dependence Ψ_t and the salinity dependence Ψ_s to the absorption coefficient α [40]

$$\Phi = \alpha + \Psi_t(t - 273.15) + \Psi_s C_s . \tag{2.2}$$

The temperature and salinity corrected absorption coefficient Φ is introduced in Equation (2.2). The absorption coefficient α for a wavelength of 620 nm in salt water at 20 ^{o}C is 0.002755 m^{-1} [32]. The temperature dependence Ψ_t is 0.000539 m^{-1} ^{o}C^{-1}, and the salinity dependence Ψ_s is 0.0000838 m^{-1}g^{-1}L for a wavelength of 620 nm as provided by Rottgers et al. [41]. Substituting these values into Equation (2.2), we get the corrected absorption coefficient at 620 nm as

$$\Phi_{620} = 0.002755 + 0.000539(t - 273.15) + 0.0000838 \times C_S . \tag{2.3}$$

The water temperature t is give in Kelvin and C_s is the salt concentration of the water in g/L.

The properties of light propagation in the ocean water are the basis of the development of the techniques for estimating depth in three dimensions (3D) underwater scenes.

THIS PAGE INTENTIONALLY LEFT BLANK

III. DEVELOPMENT OF PROPOSED TECHNIQUE

The natural properties of light described in Chapter II may be used to compare two underwater images to provide a three-dimensional representation of the environment surrounding the AUV. This technique not only does not require significant processing power but is also passive and does not require energy sources, such as sound or artificial light. A camera, filter, and natural light are all that are required.

Accurate results do require the temperature and salinity to be known, and they are highly dependent on turbidity, or the concentration of particulate in the water. This method is considered a type of visual odometry because it analyzes camera images to process an environment. The temperature and salinity corrected absorption coefficient Φ has been substituted into Equation (2.1) and rearranged to solve for a distance d:

$$d = -\left(\frac{1}{\Phi}\right)\ln\left(\frac{I_d}{I_o}\right). \tag{3.1}$$

If precise wavelength-specific luminous intensities can be obtained just below the surface of the ocean I_{oA} and at the subject I_A then the depth of the object d_A may be determined based on Equation (3.1) as shown in Figure 3. A form of Equation (3.1) is often used in determining where light-dependent organisms may be found based on their food requirements [42]–[44]. Similarly, if the wavelength-specific luminous intensities can be obtained at the subject I_{oB} and at the camera I_B, then the distance from the subject to the camera d_B can also be determined from equation (3.1), also shown in Figure 3. The total distance that the light has traveled through the water includes the depth of the object and the range to the object: $distance = depth + range$. This corresponds to adding d_A and d_B from Figure 3 together to get the total distance the light has traveled through the water.

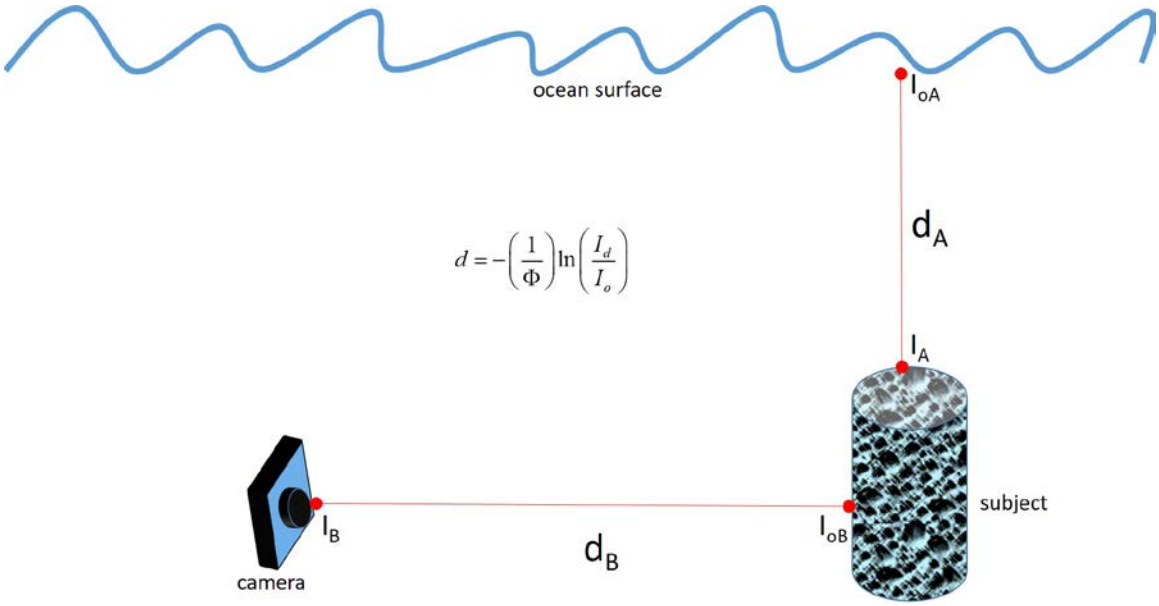

Figure 3. Image Showing Distances from Surface to Subject and to Camera

If the light intensity decays at the same rate with distance, then the color will appear the same but with decreased brightness (lower luminous intensity). As described by the Beer-Lambert law in Chapter II, the light intensity at different wavelengths experience different exponential decays and is perceived as a shift in color from reds to blues and greens.

An image is stored as a three-dimensional matrix of RGB values, which together describe a color for each pixel. As light travels through the water, these RGB values decay toward the green-blue side of the color triangle. An observer, or in this case a camera, sees a different color because the wavelength-specific luminous intensities decay unevenly causing the color shift. As the red is absorbed first there is a shift in color towards blue and green. Studying the shift in color provides some useful information that is comparable to using the luminous intensities.

Filters are widely used in underwater photography. They are designed to correct for the shift in color. Filters work by blocking some wavelengths (mostly blues and greens) from reaching the camera sensor. They do not entirely block these wavelengths but allow more red wavelengths to reach the camera to help restore the balance of color. Blocking some of the blue and green wavelengths causes a shift in color back toward a

natural balance of colors. Restoring the balance of color comes at a cost. By blocking some of the light, the image appears darker, but the colors appear more natural.

Filters are also limited in use by the decay of the red wavelengths. At deeper depths or when photographing subjects that are farther away, the red wavelengths decay entirely and the filter is not useful. An image captured with a filter will appear as close to the correct color, although at a lower intensity, because the RGB values for each pixel have been restored to a proper balance. The filtered image may be used as the initial color or the properly balanced color, while the unfiltered image shows how much the color has shifted over an unknown distance. The Beer-Lambert law uses light intensities to determine a range. Having the proper color representation does not give the proper luminous intensity. Determining how much the color has shifted only provides a relative distance between objects in the image when used in Equation (3.1) rather than an absolute distance from the camera to the objects.

Most visual and laser based methods of underwater ranging prefer a wavelength that has the least attenuation. Choosing light in the blue-green region ensures that the light will travel farther, thus illuminating objects farther away or providing a higher chance of reaching the collector. For this technique, light in the red region is used because it has the highest attenuation over a short distance. This is done to create the highest contrast between the initial intensity and final intensity over the smallest distance or, in this case, the greatest color shift over the smallest distance.

The blue and green wavelengths experience a much slower exponential decay. They are assumed to remain constant over the short distances analyzed. An RGB value of (1,0,0), corresponding to a wavelength of 620 nm (bright red), is selected as a reference for convenience because it is on one corner of the RGB color space. This wavelength is known to rapidly decay towards the blue-green side of the triangle in Figure 2, so it provides some color shift. For example, a pixel with a value of (1,0,0) indicates that no red has been lost; therefore, the object has to reflect red (the object has red (1,0,0) or white (1,1,1) in its color) and be directly in front of the camera and just beneath the surface (no loss due to absorption). If that object is moved down the water column or

away from the camera, then it experiences a color shift. Measuring that color shift reveals how far the light has traveled underwater.

The difference in red pixel values between two images, one filtered and the other unfiltered, taken at the same location may be used to determine the relative distance between objects within the frame. Substituting filtered and unfiltered red pixel values for initial and final intensities into Equation (3.1), we get

$$d_r = -\left(\frac{1}{\Phi}\right)\ln\left(\frac{R_u}{R_f}\right), \tag{3.2}$$

where R_u represents the R matrix in the unfiltered image, R_f is the R matrix in the filtered image, and d has been replaced with d_r to denote a relative distance between objects within the image.

A boundary condition occurs when the filtered pixel value contains no red (0,0,0) because taking the natural log of 0 yields -∞. This indicates one of two situations, either there was no red reflected from the object (the initial intensity for red wavelengths was 0) or all of the red wavelengths have fully decayed (the light has traveled far enough to fully decay).

In the next chapter we demonstrate the effectiveness of this technique by applying it to a number of different depth and range conditions.

IV. EXPERIMENTAL DESIGN AND DATA COLLECTION

This new technique is dependent on colors and specifically comparing colors between images. Using different cameras to take some of the images or using different computers to process the results may introduce unnecessary error because of different RGB color spaces; therefore, all images were collected using the same camera setup in the same general location by the same operator over consecutive days to reduce variations. All processing was done on the same computer using the same version of software.

A. EQUIPMENT SELECTION AND SETUP

Initially, data collection was attempted in a tank and a pool. Data collection in a tank offered the challenge of controlling the light source. The tank had glass on all sides which allowed light in from all angles, preventing successful data collection. The glass also has some absorbance which would have affected the results; therefore, a tank is not desirable for data collection. A pool was also attempted. Light only penetrated the surface of the water; however, most pools, including the one used, are painted white, which allows significant reflection from the bottom and sides. The reflectivity of light underwater from surfaces such as a sandy bottom has been studied previously by Lee et al. [45], Mobley et al. [46] and English and Carder [47]. The reflectivity of the light off the bottom and sides of a white pool significantly impacts the results and is also not desirable.

Further investigation of a suitable location to gather data suggested a gently sloping ocean floor at depths of 5–12 m with visibility that exceeded 20 m to ensure absorption of the desired wavelength dominated rather than scattering. A sandy bottom would also result in reflection like in the pool, so a rocky bottom is preferred. A high tidal current and large sea state will cause difficulty in obtaining proper images, so an area with low current is preferable. After careful consideration, a location on the West side of Oahu in the Hawaiian Islands was selected.

A GoPro Hero 4 was selected as a camera. The Hero 4 is easy to use, records high quality High Definition (HD) video, and is easily accessible. It was mounted on a tripod and taken to depths of 5–10 m of water and placed at various distances from natural and manmade objects. Video footage was taken at each location with two filters (Flip4 "Dive" and "Deep") and without a filter. Data was collected during five dives over a two-day period at various times of day and night. Diver one set up the tripod and operated the filters during all data collection. Diver two measured the distance to a known object for reference for each dataset. Video footage was processed using Pinnacle 19 to obtain still images. Images were cropped to ensure each pair of filtered and unfiltered images had the same field of view. A filtered image and the corresponding unfiltered image were processed as a pair using MATLAB R2015b Image Processing toolbox and user generated code found in the Appendix.

Water temperature, salinity, and density were measured using an RBR Concerto as shown in Figure 4. Averages for each dive were calculated and compiled in Table 2. A temperature of 27.55 ^{o}C was used as the average temperature, 34.60 PSU, or g/kg, was used as the average salinity, and 22.27 kg/m^3 was used as the average density.

Figure 4. RBR Concerto Used to Measure Temperature and Salinity.
Source: [48].

Table 2. Averaged Data from RBR Probe

	Temp	Salinity	Density	C_s
Dive #	^oC	PSU	kg/m^3	g/L
1	27.41805	33.84613	21.73631	0.73569
2	27.72177	34.70507	22.28743	0.773487
3	27.5493	34.7634	22.38712	0.778252
4	27.42537	34.75553	22.42119	0.77926
Average	27.54915	34.60401	22.26674	0.770519

Using these average values in Equation (2.3) produces a temperature and salinity corrected absorption coefficient of 0.00689 m^{-1}. Substituting this into Equation (3.2) produces

$$d_r = -0.14517 \ln\left(\frac{R_u}{R_f}\right), \tag{4.1}$$

with the relative distance d_r given in mm. Image pairs were captured as described above producing a pair of RGB matrices. The emphasis of this experiment is to get range information for short distances (less than 10 m) so the analysis focuses on the R matrices. For each (x,y) pixel, the R value from the unfiltered image was divided by the R value from the filtered image. This produced a new matrix of relative distances for each (x,y) pixel value. This matrix is represented as a three-dimensional wire-mesh with colored peaks indicating distances.

A dark blue indicates a low value or no object detected. A bright yellow indicates a high value or close object. These are still relative values, so a bright yellow object may not be close though it may be closer than all other detected objects. The boundary condition mentioned above creates unnecessary peaks which may skew the results. As a result, code was added to search for pixels whose value exceed a threshold, and those pixels were set to a nominal value to avoid skewing the results.

B. DATA PROCESSING

The theoretical maximum distance $D_{max,t}$ traveled by red wavelengths of light in clear water is 10 m. The first pair of images (Figure 5 and Figure 6) were taken at a depth

of 8.3 m and approximately 2.0 m from the subject to the camera, so the light has traveled a total of 10.3 meters through the water. This image pair is, therefore, near the theoretical maximum distance for red light.

An unfiltered image taken approximately 2.0 m from the subject at a depth of 8.3 m is shown in Figure 5. This image represents a matrix of light that has lost intensity and experienced a color shift as the light has traveled from the surface to the subject and from the subject to the camera. This matrix does not accurately depict the change in luminous intensity but rather the shift in color as the wavelengths of light have been absorbed. This image appears to be washed out, mostly showing greens and blues and is common among amateur underwater photographers.

Figure 5. Unfiltered Image 8.3 m Deep, Range of 2.0 m to Subject

A filtered image is shown in Figure 6 that was taken from the same location as the image in Figure 5. This image represents a close approximation of the original colors of the subject. This does not accurately represent the initial luminous intensities from the Beer-Lambert Law but instead represents the color balance restored by using the filter.

Figure 6. Filtered Image 8.3 m Deep, Range of 2.0 m to Subject

By subtracting the unfiltered image from the filtered image, we see how the filter altered the image. A pixel-by-pixel subtraction of Figure 5 from Figure 6 produces the results shown in Figure 7.

Figure 7. Image Showing Difference between Figure 5 and Figure 6

After fully processing the images, the results are displayed as a 3D wire-mesh in Figure 8 and Figure 9. For each (x,y) pixel in the image, a value is given to describe the relative distance. A brighter yellow (taller peak) shows objects that are closer, while darker blues (valleys) show objects that are farther away. The coral is visible with yellow peaks indicating where the coral sticks out farther or is closer to the camera. The lines of raised iron are also visible on the right-hand side of the image indicating where the wall protrudes. This can also be converted to a 3D point cloud for use in navigating underwater vehicles.

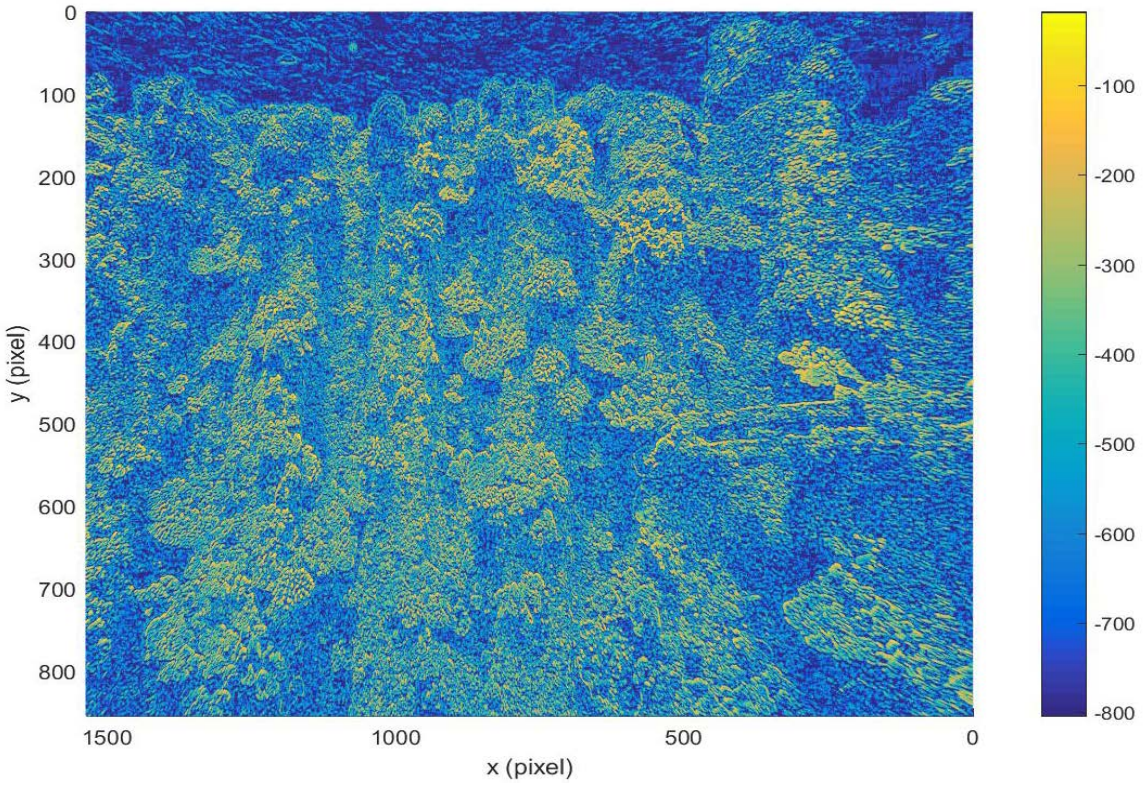

Figure 8. 3D Representation of Figure 5 and Figure 6

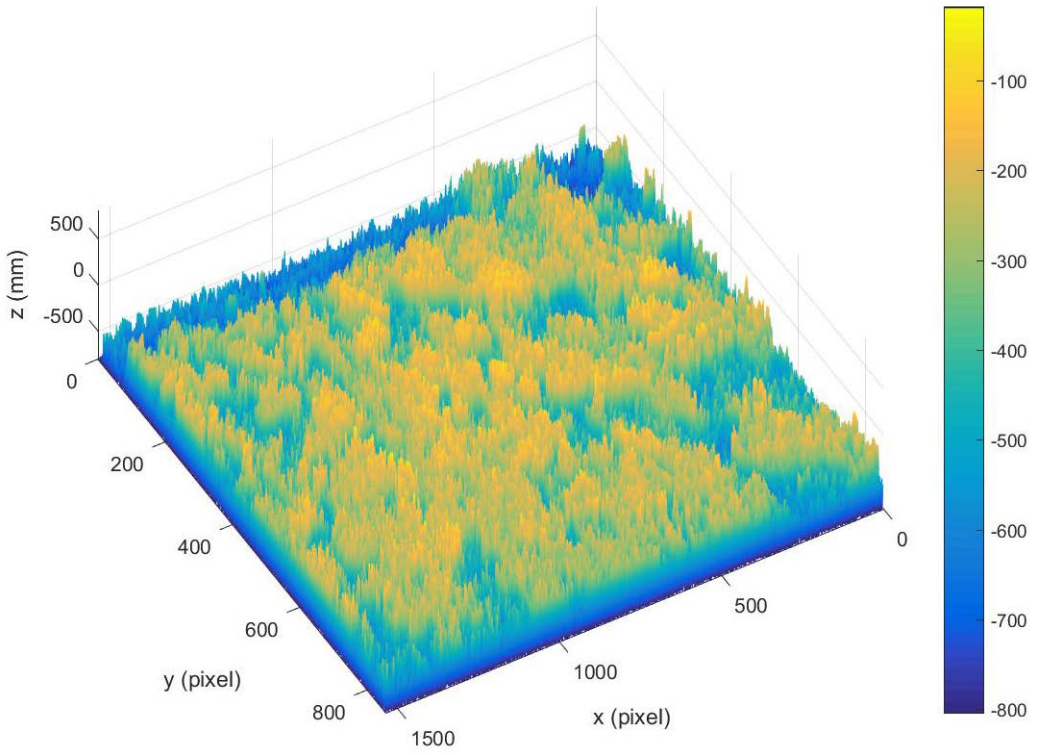

Figure 9. 3D Representation of Figure 5 and Figure 6 Rotated to Show Depth

Zooming in on specific features, such as the coral in the middle of the image near the top of the wall, demonstrates the resolution of this technique. The post-processed image and the filtered image are shown in Figure 10 for comparison. It is easy for the human eye to imagine the coral protruding in a photograph but difficult to quantify how far it protrudes. It is even more difficult to convey this obstacle to an underwater vehicle. This technique can quantify these objects and be used in navigating an underwater vehicle.

The same subject photographed at a range of 5.0 m and a depth of 8.3 m is shown in Figure 11 and Figure 12. Adding these distances together gives a total distance of 13.3, which is 33% larger than the theoretical maximum distance $D_{max,t}$ that the red wavelengths can travel. The expected result is less resolution because some of the filtered pixel values have reached zero. The unfiltered image is shown in Figure 11, and the filtered image is shown in Figure 12.

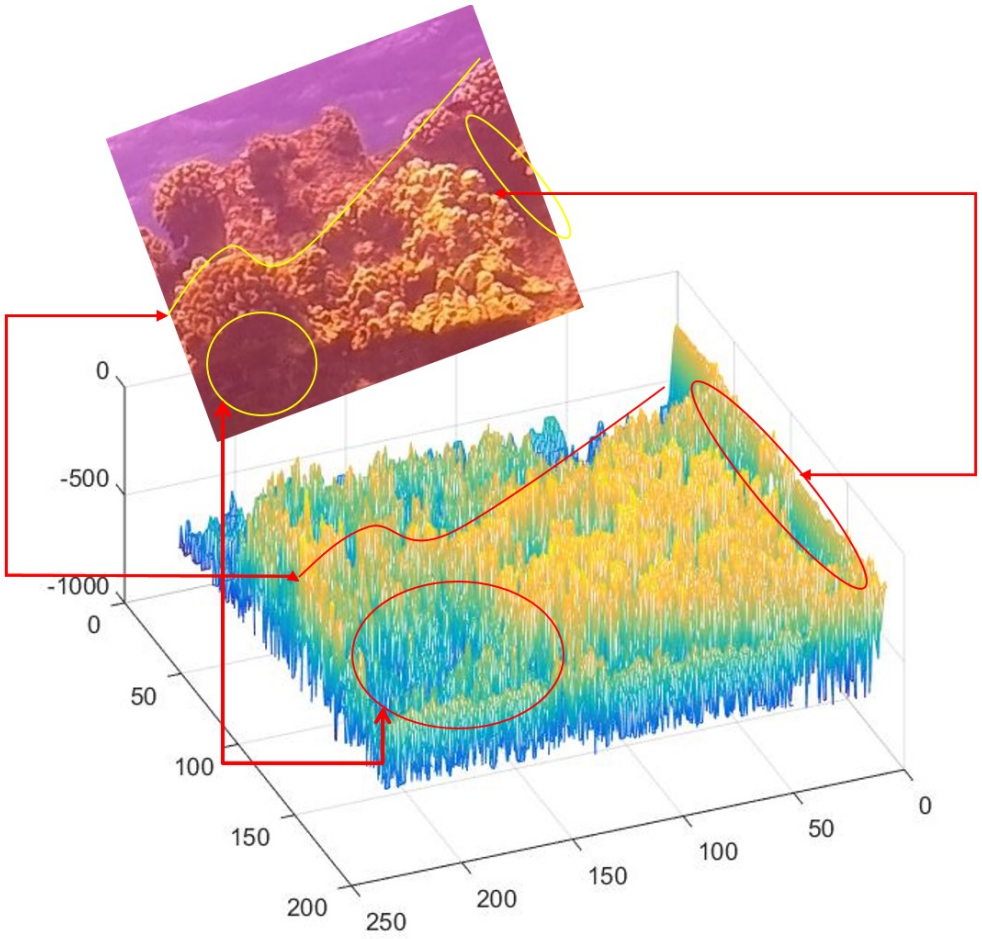

Figure 10. Comparison of Processed 3D Image of Coral to Original Coral Image with Features Highlighted

Figure 11. Unfiltered Image 8.3 m Deep, Range of 5.0 m to Subject

Figure 12. Filtered image 8.3 m Deep, Range of 5.0 m to Subject

As expected, the same wall photographed at 5.0 m shows significantly less resolution than the images at 2.0 m even when cropped to cover the same area. All the intensities have decreased as the light has traveled farther through the water. With a lower overall intensity, it is more difficult to distinguish details within the remaining values. This can be seen in Figure 13. The image appears darker overall.

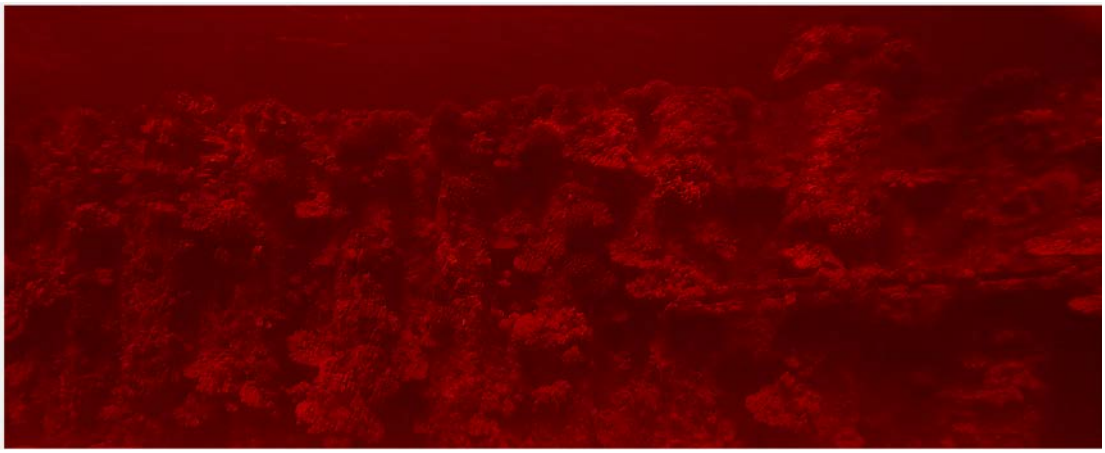

Figure 13. Image Showing Difference between Figure 11 and Figure 12

There are many pixels that reflected red light, but much of that light does not make it to the camera such that even with the filter they appear as (0,0,0), or far away. This can be seen in the final processed image in Figure 14 and Figure 15.

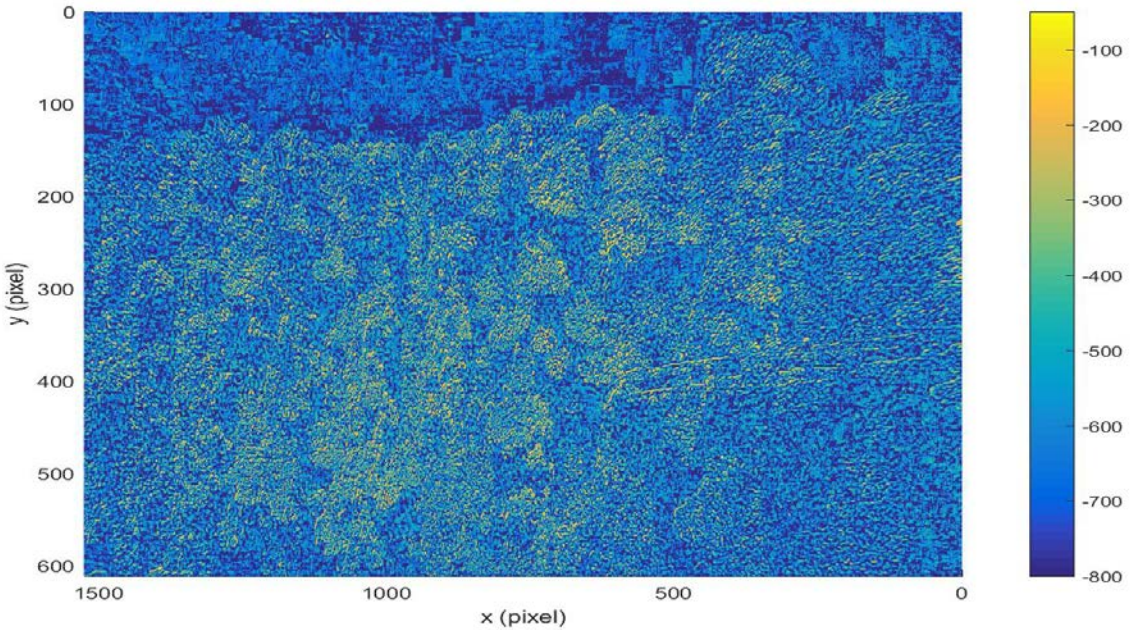

Figure 14. 3D Representation of Figure 11 and Figure 12

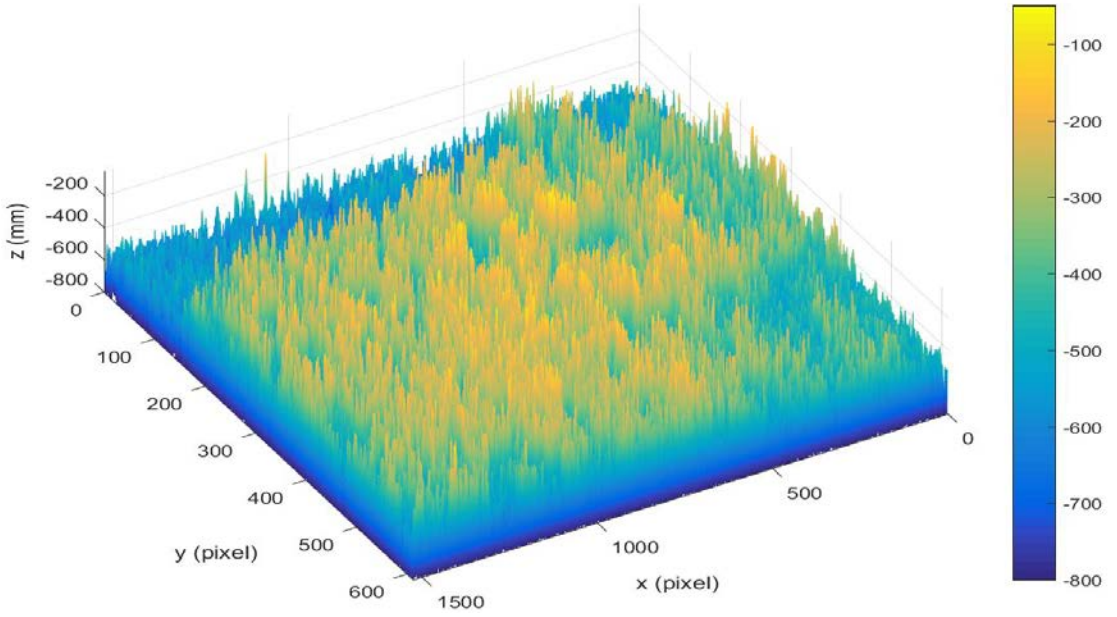

Figure 15. 3D Representation of Figure 11 and Figure 12 Rotated to Show Depth

When comparing the features in Figure 10, this same coral has significantly less resolution as seen in Figure 16. The same features are still visible but less prominent. Some red did still reach the camera, so 13.3 m is not an absolute maximum for the red wavelengths to travel. It does indicate that using red wavelengths is less accurate at this distance.

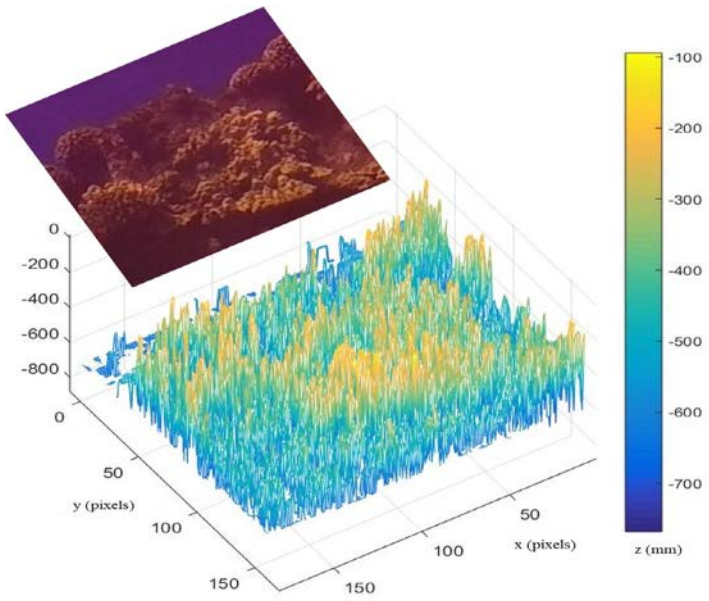

Figure 16. Comparison of Processed 3D Image of Coral with Original Coral Image

There exists a local maximum distance $D_{max,l}$ which depends on the temperature and salinity as well as the particulate concentration. This local maximum may be significantly smaller than the theoretical maximum, especially because of higher particulate concentration. The local maximum where this technique remains effective lies somewhere between 10.3 m and 13.3 m. This local limit can be quantified with further experimentation but will vary by location and conditions. In situations where high resolution may be sacrificed for speed, this level of accuracy may be sufficient. To navigate an underwater vehicle, it may be sufficient to know that there is an object present without knowing the detailed features of the object.

Images taken at deeper depths must be closer to the objects to remain inside the local maximum $D_{max,l}$. An object photographed at 2.0 m and a depth of 10.0 m is shown in Figure 17 and Figure 18. This means that the total distance the light has traveled underwater is 12.0 m which is still 20% larger than the theoretical maximum distance $D_{max,t}$. This image pair shows less contrast like the images shown in Figures 11–15. An unfiltered image taken 2.0 m away at a depth of 10.0 m is shown in Figure 17, and the corresponding filtered image is shown in Figure 18.

Figure 17. Unfiltered Image 10.0 m Deep, Range of 2.0 m to Subject

Figure 18. Filtered Image 10.0 m Deep, Range of 2.0 m to Subject

Subtracting the image in Figure 17 from the image in Figure 18 produces Figure 19, which shows the effect of the filter. This image is darker, like Figure 13.

Figure 19. Image Showing Difference Between Images in Figure 17 and Figure 18

The processed image from a depth of 10.0 m and a range of 2.0 m is shown in Figure 20 and Figure 21. The outline of the subject is clearly visible, but there is not as much depth to the 3D image as there was in Figure 8 and Figure 9. The fish standout as the closest (and perhaps the brightest colored) objects in the frame.

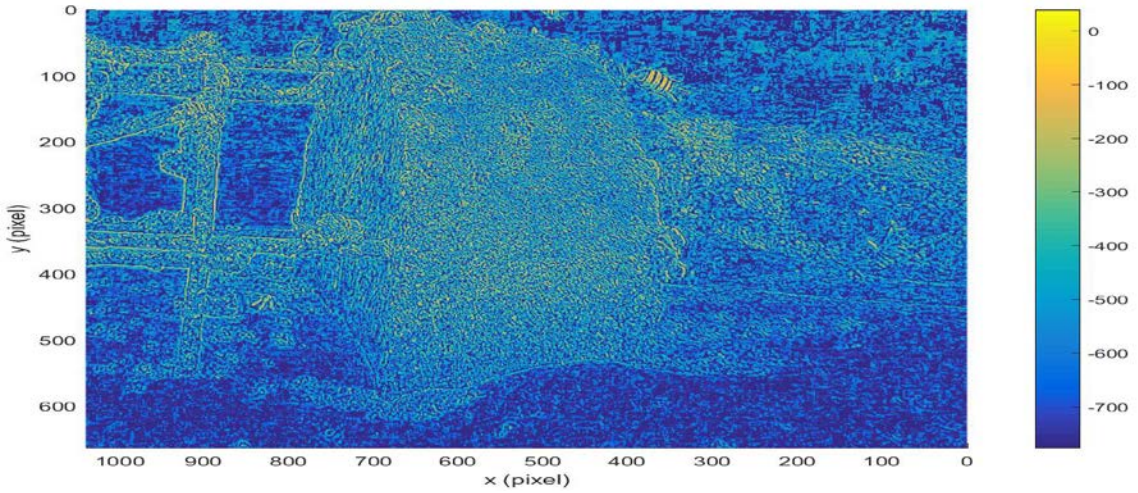

Figure 20. 3D Representation of Figure 17 and Figure 18

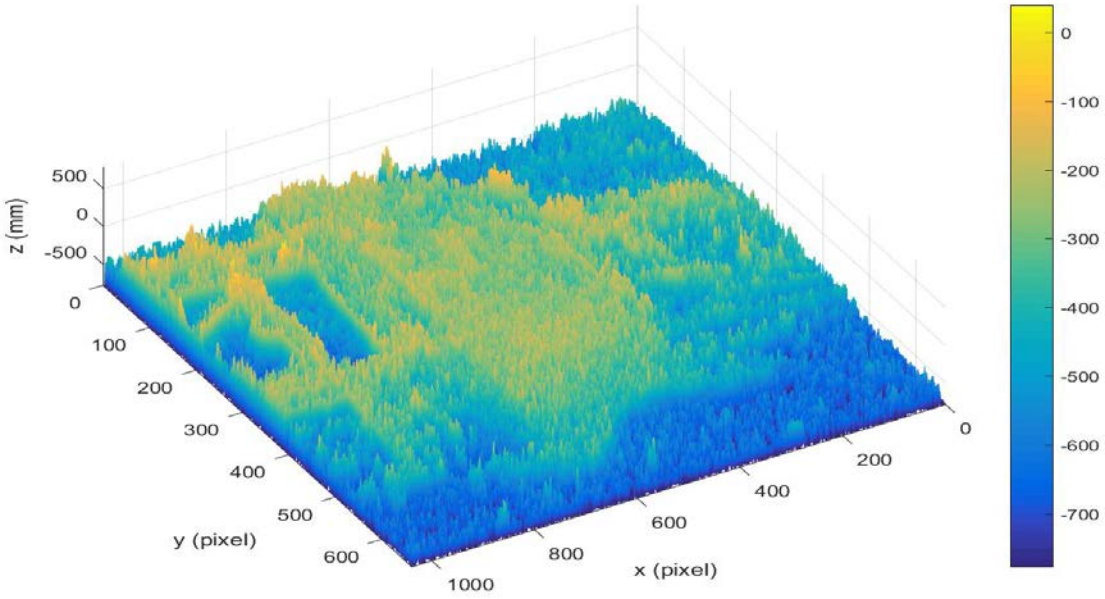

Figure 21. 3D Representation of Figure 17 and Figure 18 Rotated to Show Depth

Images taken at a shallower depth (5.0 m) and range of 2.0 m are compared in Figures 22–26. The unfiltered image at this depth and range combination is shown in Figure 22 with the corresponding filtered image shown in Figure 23.

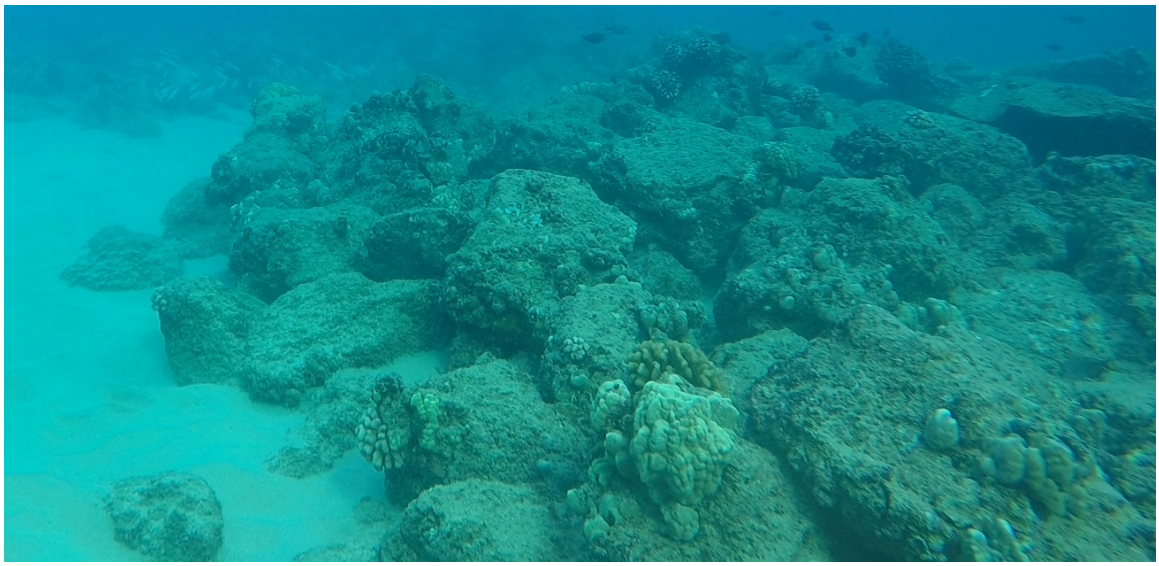

Figure 22. Unfiltered Image 5.0 m Deep, Range of 2.0 m to Subject

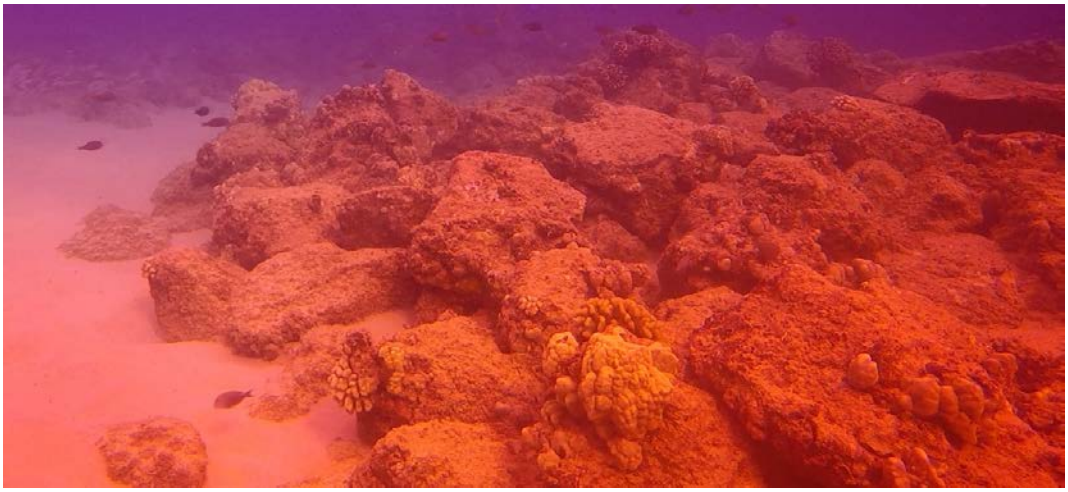

Figure 23. Filtered Image 5.0 m Deep, Range of 2.0 m to Subject

At this depth and range, the total distance should be well within the theoretical maximum distance $D_{max,t}$. Indeed, processing this image pair yields good contrast between objects in the frame as seen in Figures 24 and 25. This contrast appears to be better than that in Figure 8 because the red light has not traveled as far. There is, however, some saturation evident in the lower left quadrant of Figure 24. This area has been blown up to show the detail in Figure 26. The reflectance from the sand is visible, causing a "false return." This was anticipated when analyzing images with significant amounts of sand visible as predicted by English and Carder [47].

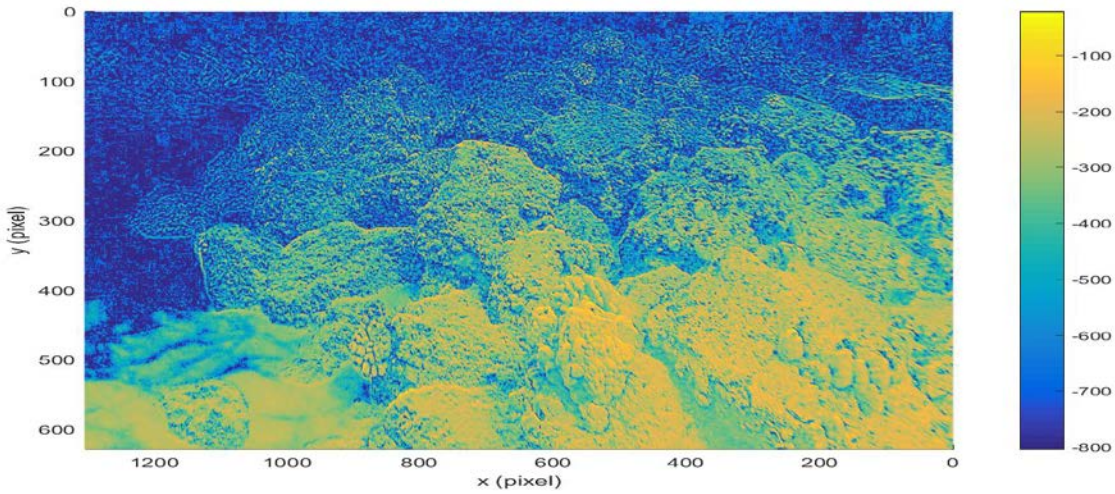

Figure 24. 3D Representation of Figure 22 and Figure 23

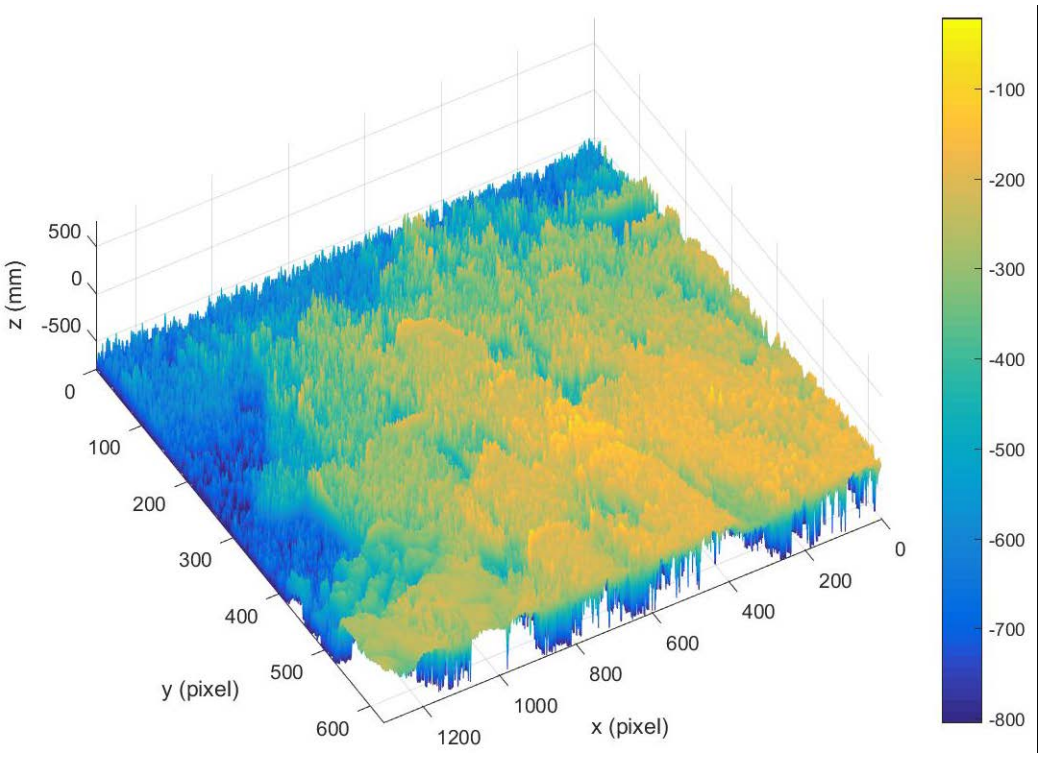

Figure 25. 3D Representation of Figure 22 and Figure 23 Rotated to Show Depth

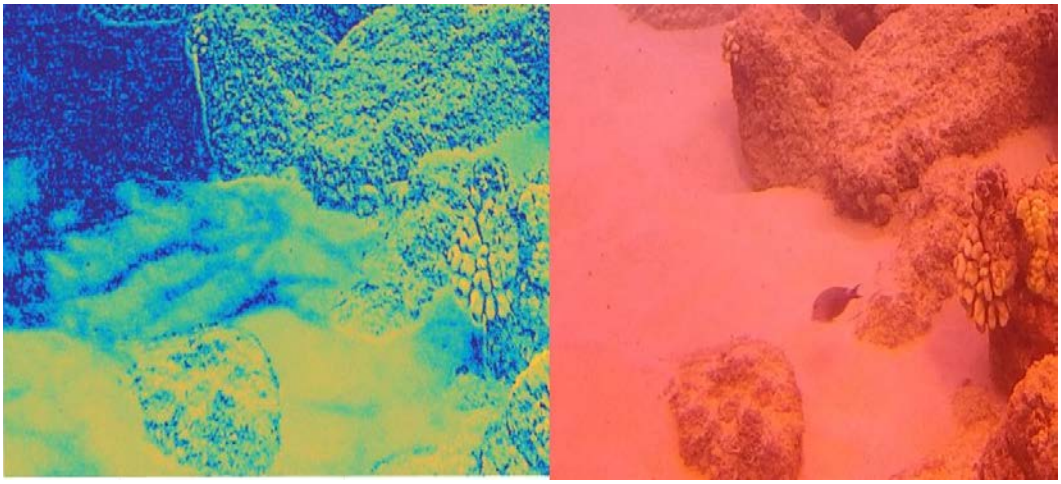

Figure 26. Exploded View of Lower Left Corner of Figure 24 Compared to the Original Filtered Image in Figure 23

Images taken at a depth of 5.0 meters and range of 8.3 meters from the subject are shown in Figure 27 and Figure 28, respectively. This distance is known to be outside the local maximum $D_{max,l}$ but presents some interesting information. The unfiltered image is shown in Figure 27, and the corresponding filtered image is shown in Figure 28.

Figure 27. Unfiltered Image 5.0 m Deep, Range of 8.3 m to Subject

Figure 28. Filtered Image 5.0 m Deep, Range of 8.3 m to Subject

The processed image from the pair shown in Figures 27 and 28 is shown in Figure 29. The bottom reflectance from the sand is again visible across the bottom in Figures 29 and 30. Additionally, the line used to measure distance to the objects did not clear the picture and shows up as a bright yellow line on the right-hand side of the image. It is, in fact, the closest object in the image and is also red in color. The limitation of using a red wavelength is also visible as the coral in the middle of the raw images does not appear in the processed image. There is a distinct gradient seen along the right-hand side of the image. Objects in the lower right-hand corner are within the local maximum $D_{max,I}$. and appear to have decent contrast. Objects that are farther away start to lose contrast and eventually fade from view.

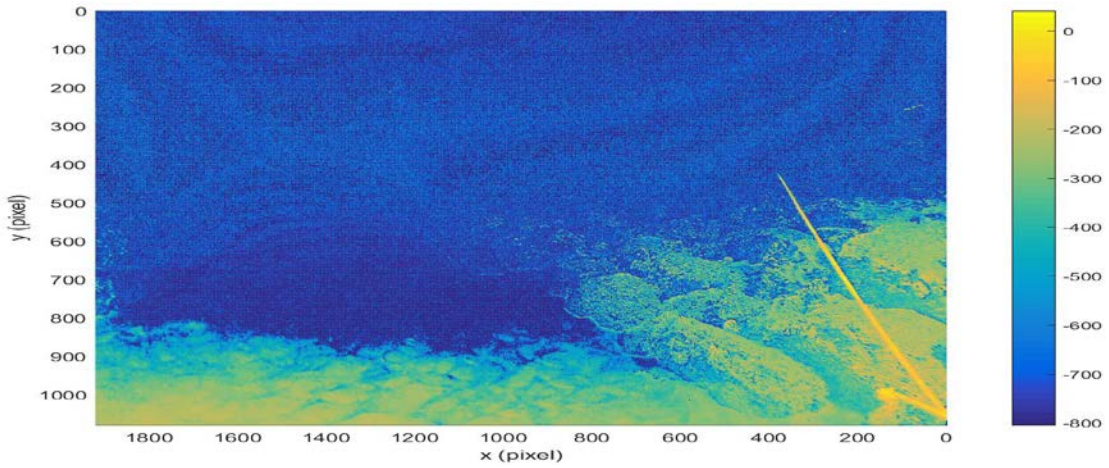

Figure 29. 3D Representation of Figure 27 and Figure 28

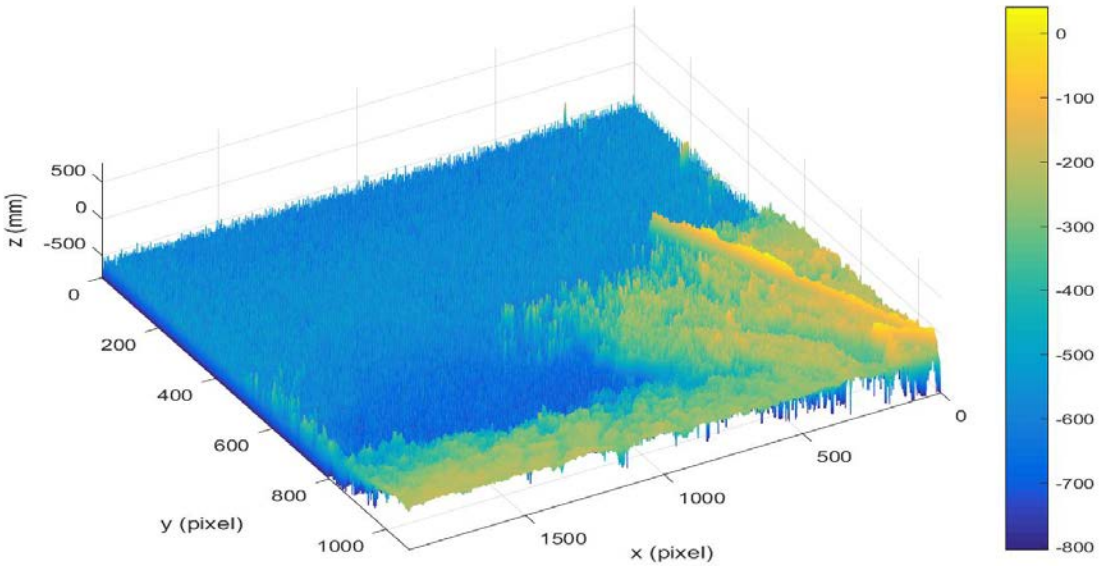

Figure 30. 3D Representation of Figure 27 and Figure 28 Rotated to Show Depth

Another observation from this image is that with significant visible water overhead it is possible to see striations in the water due to the flat port used to capture the images. This may be due to the polarized nature of light in water as previously studied by Cronin and Shashar [49] and many others.

C. GREEN AND BLUE MATRIX ANALYSIS

Similar analysis was performed on the green and blue matrices from the images in Figures 5 and 6. The temperature and salinity corrected absorption coefficients for the other two corners of the Adobe RGB triangle, green (510 nm) and blue (440 nm), were calculated using Equation (2.3) and data provided by Rottgers et al. [41]. Results are shown in Table 3 for all three wavelengths.

Table 3. Temperature and Salinity Corrected Absorption Coefficients. Adapted from [32], [41].

	Wavelength		
	440 nm	510 nm	620 nm
α (1/m)	6.35×10^{-3}	3.25×10^{-3}	2.76×10^{-3}
ψ_S (1/m*L/g)	2.22×10^{-5}	1.75×10^{-6}	8.38×10^{-5}
ψ_T (1/m*1/K)	2.96×10^{-6}	7.71×10^{-5}	5.39×10^{-4}
$\phi = \alpha + \psi_T(t - 273.15) + \psi_S(C_s)$			
ϕ (1/m)	6.39×10^{-3}	3.31×10^{-2}	6.89×10^{-3}

The values from Table 2 may be substituted into Equation (3.2) for Φ_{510} and Φ_{440} to obtain

$$d_r = -30.23 \ln\left(\frac{G_u}{G_f}\right) \tag{4.2}$$

and

$$d_r = -156.51 \ln\left(\frac{B_u}{B_f}\right), \tag{4.3}$$

where G_u represents the green pixel values from the unfiltered image, G_f represents the green pixel values from the filtered image, B_u represents the blue pixel values from the unfiltered image, and B_f represents the blue pixel values from the filtered image.

The green and blue matrices were analyzed using Equations (4.2) and (4.3) similar to the way the red matrix was analyzed with Equation (4.1). As expected, the matrix of green values shows very little change over a short distance, as seen in Figure 31.

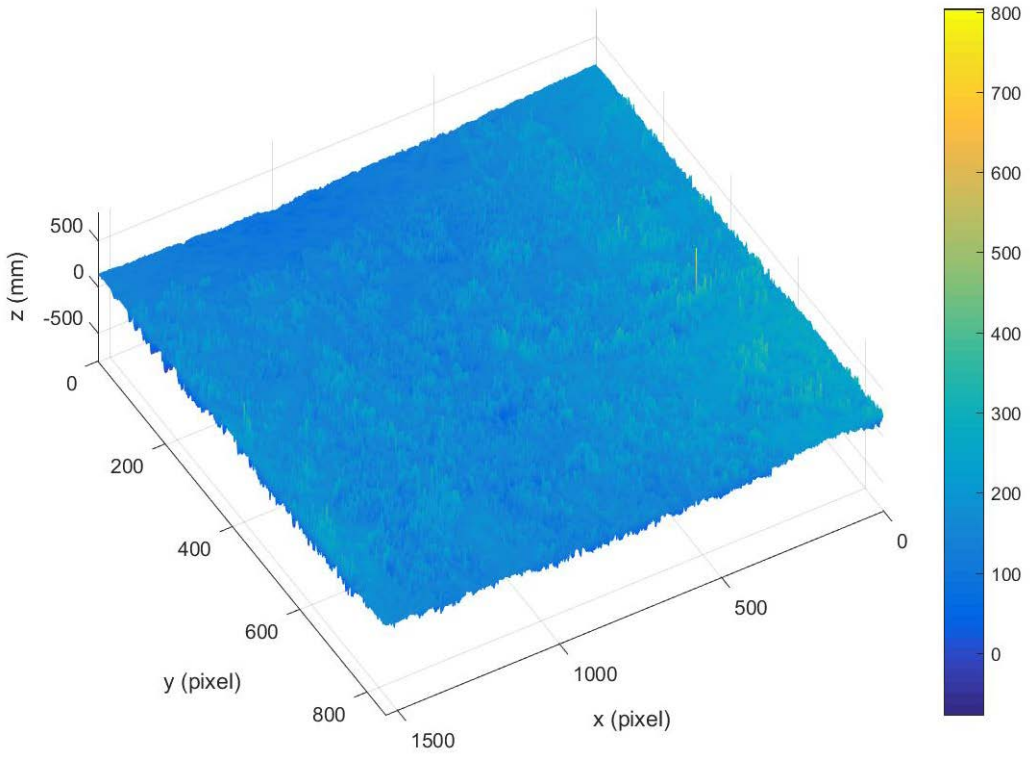

Figure 31. 3D Representation Based on the Green Pixel Values from Figures 5 and 6

There is a surprisingly large color shift in the blue matrix values for this image pair as seen in Figure 32. In this image it is easier to distinguish the open ocean above the coral from the edge of the coral. The results from the blue matrix may be better than the results from the red matrix in determining a safe place for navigating an underwater robot in this case. The higher wavelengths seem to experience significant absorption over short distances, especially the purples and deep blues as seen in the left-hand side of Figure 16. This shows that both the red and blue corners of the Adobe RGB triangle shift toward the green corner in Figure 17.

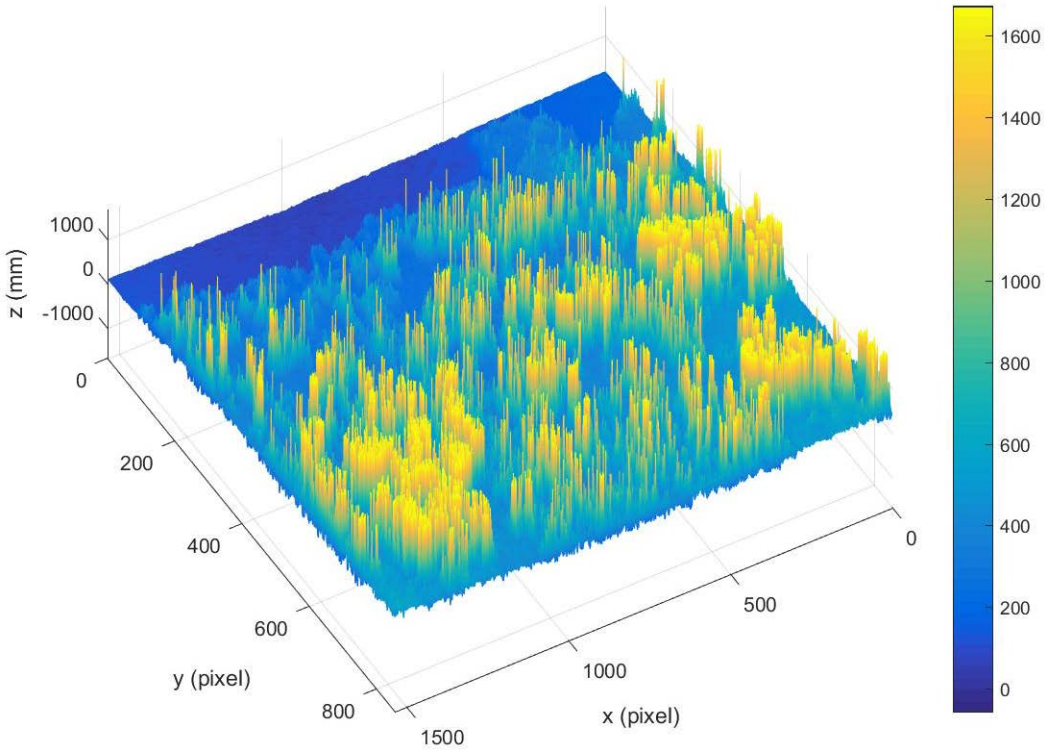

Figure 32. 3D Representation Based on the Blue Pixel Values from Figures 5 and 6

Comparing the results from analyzing the green and blue matrices for the images in Figure 27 and 28 taken at a depth of 5.0 m and range of 8.3 m produces the 3D representations shown in Figure 33 and Figure 34, respectively. The red line used to measure distances is no longer dominant and is now barely visible. The bottom reflection from the sand is also notably absent. The green matrix provides little value, but the blue matrix shows the coral on the left-hand side of the image as well as the coral in the middle of the image that did not show up when analyzing the red matrix.

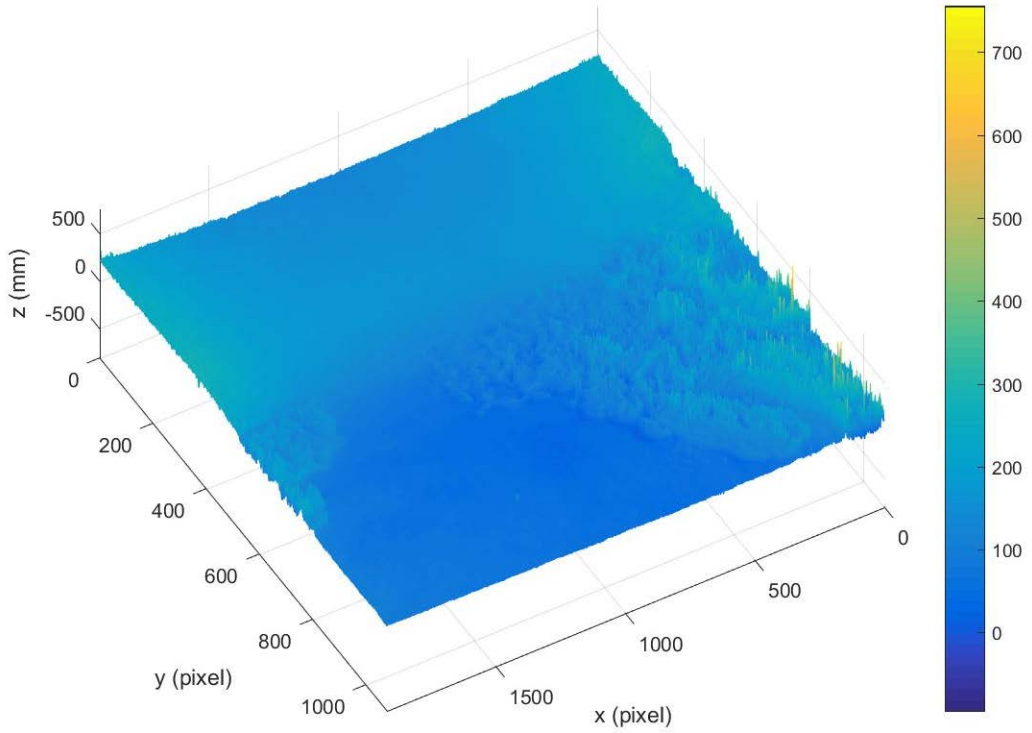

Figure 33. 3D Representation Based on the Green Pixel Values from Figure 27 and Figure 28

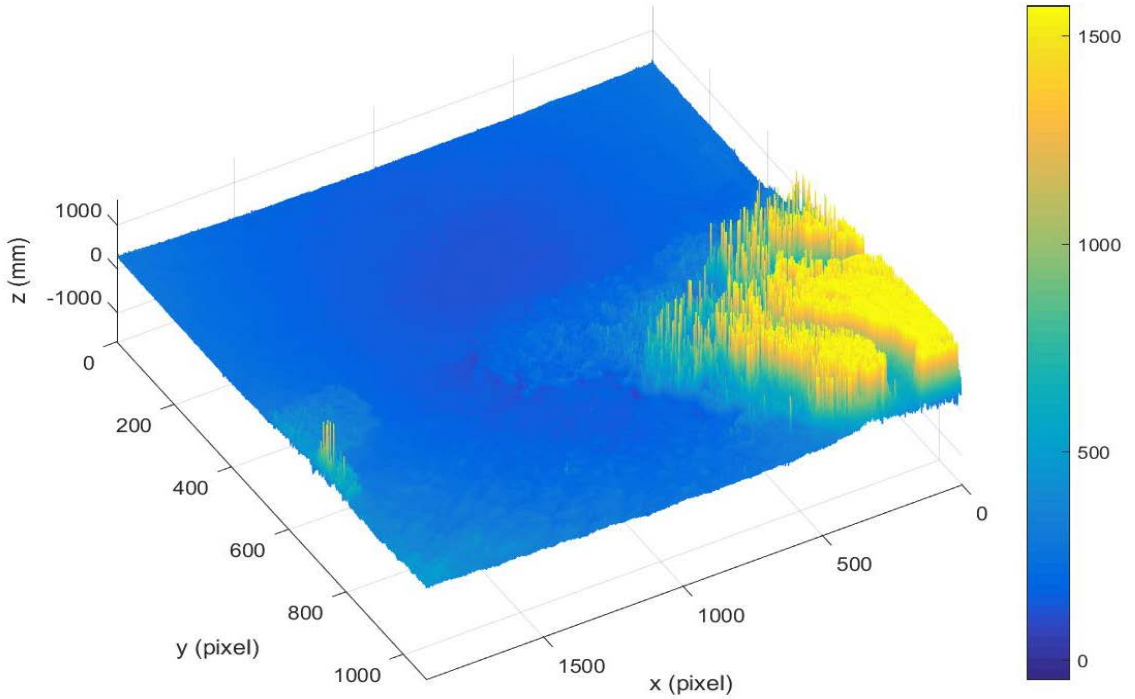

Figure 34. 3D Representation Based on the Blue Pixel Values from Figures 27 and 28

As previously mentioned, the RGB color space adds red, green, and blue values to produce a color. Splitting a color into its red, green, and blue components allows analysis of how each one changes as it passes through water. The green component changes very little, as expected, because its exponential decay is significantly slower than the other two. The blue and red components both provide useful information in analyzing a scene. Adding the 3D results from analyzing the red, green, and blue matrices back together to reform an RGB representation produces little added value and is not recommended, as seen in Figure 35.

This image shows a comparison of green (a), blue (b), red (c), and a combination of red + green + blue (d) 3D representations of Figure 10. It is clear from the blue matrix in Figure 35(b) where the clear blue water is compared to the coral. The outline of individual coral is more visible from the red matrix in Figure 35(c). Combining the images make everything less visible as seen in Figure 35(d).

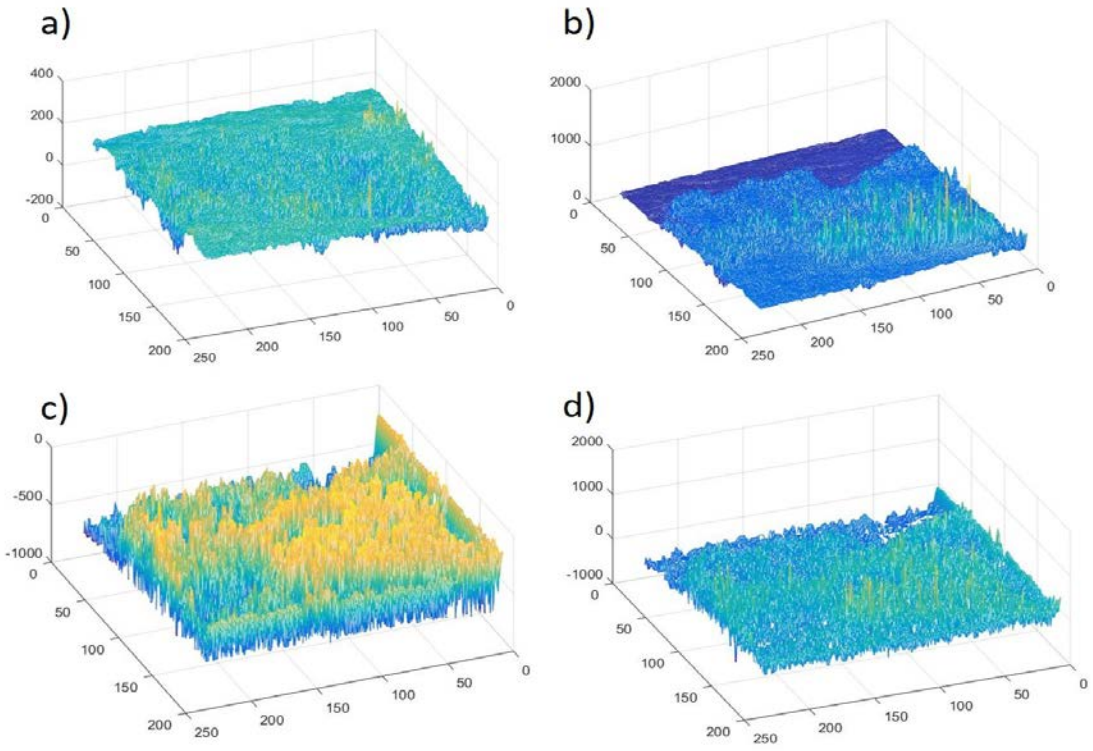

Figure 35. 3D Representations of Figure 10 Using Green (a), Blue (b), Red (c), and Red + Green + Blue (d) Values

V. CONCLUSIONS AND RECOMMENDATIONS

A. CONCLUSIONS

A new technique has been developed for improving underwater robot vision. This technique is vision-based and only requires a camera, a filter, and sufficient natural light. By comparing two raw images, one filtered and one unfiltered, we can generate a detailed three-dimensional image showing the relative distance between objects in a scene. This is done by separating the color in each pixel into its respective red, green, and blue values. The red and blue values shift toward the green corner in the RGB color space as the light travels through water. Analyzing the amount these values shift approximates relative distances between objects in the frame. It is possible to capture and process these images to determine these relative ranges using commercially available equipment.

Absolute ranges from a vehicle to objects in a scene are more important and were the original intent of this work. This technique alone cannot determine absolute ranges but does provide useful information and can still be used to provide robot vision. This technique can also be combined with other sensors or techniques and further develop into absolute ranges. For example, it can be combined with a single-point laser rangefinder. Knowing the absolute range to a single point reveals the range to all other points based on the relative ranges provided by this technique. Another possibility is to employ this technique in stereo or in combination with motion. Comparing results between two cameras with known spacing may provide additional range information. Similarly, processing sequential images and analyzing the optical flow field may also provide additional range information. This is known as egomotion [18].

A red wavelength was chosen based on the known properties of short-wavelengths in water. This wavelength does indeed provide useful relative range data for a given scene. Analyzing the blue wavelength also provides useful data and should also be used to establish robot vision. The green wavelength is not useful over short distances but may prove useful over longer distances.

The upward reflectance is a significant issue for areas with a sandy bottom. Analyzing the change in blue values may be able to counter this negative effect. One way this may be useful is to analyze the image in sections. There are many edge detection algorithms that are suitable for processing images. These algorithms may be applied to the results from the blue analysis to determine which portions of the image should be analyzed using the red values and which portions should be ignored (open ocean, sand, etc.). For robot vision, knowing where the open ocean is compared to objects may be sufficient to establish a low level of autonomy.

In conclusion, this is an exciting new method in underwater robot vision that has not been previously attempted. Comparing an unfiltered image with a filtered image produces relative range information. Absolute ranges may be determined when combining this technique with other sensors or with future development. Red and blue frequencies are used for better ranging at short distances.

B. RECOMMENDATIONS

Additional experiments are recommended under similar conditions but with an underwater laser rangefinder. This will provide an absolute range to a single point and conceivably every point in the image. An underwater laser line scanner can also be used to verify calculations and prove this technique. Mounting multiple cameras and analyzing a sequence of images using egomotion is also recommended to provide additional depth perception to image results

Performing additional experiments are also recommended, including the use of a variety of filters at increased depths and ranges to test the limit of usability for this technique. Comparing results between similar conditions with different filters may provide additional range information or verify current calculations. Recent work has been done to develop adaptive lighting techniques that render objects as they would appear in air [29]. Comparing unfiltered images with images taken with adaptive lighting would seem to provide better results. The filtered image approximates true colors for objects underwater but is imprecise because each filter can only account for a small range of wavelengths.

Once absolute ranges can be obtained, a small form-factor apparatus should be designed to utilize this technique in real time. This apparatus should capture both filtered and unfiltered images, process the image pairs, and store or convey the results such as building a 3D point cloud. The next step would be to design a controller to drive the vehicle toward a goal. This would require a path planning algorithm using the information form the point cloud.

THIS PAGE INTENTIONALLY LEFT BLANK

APPENDIX. MATLAB CODE

```
%This program takes two images captured from the same location, one taken
%with a red filter and one without a red filter, and compares the shift in
%color. The images are processed using a form of Beer's Law as discussed in
%the paper. Results are displayed in Figures as described below.
clear all;close all;clc;
unf_img = 'Dive3_Shallow_D1_NF.jpg';
unfiltered_frame = double(imread(unf_img)); %unfiltered image
%Image taken without a filter.
unfiltered_size = size(unfiltered_frame);
unfiltered_frame = imcrop(unfiltered_frame,[0,0,unfiltered_size(2),unfiltered_size(1)]);
unfiltered_pixels = reshape(unfiltered_frame, unfiltered_size(1)*unfiltered_size(2),
unfiltered_size(3));
unfiltered = reshape(unfiltered_pixels, unfiltered_size);
fil_img = 'Dive3_Shallow_D1_F2.jpg';
filtered_frame = double(imread(fil_img)); %filtered image
%Image taken with a filter.
filtered_size = size(filtered_frame);
if filtered_size(2) ~= unfiltered_size(2)
   filtered_frame = imcrop(filtered_frame,[0,0,unfiltered_size(2),unfiltered_size(1)]);
   filtered_size = unfiltered_size;
end
%The images must be the same size for comparison. This crops the filtered
%image to be the same size as the unfiltered image.
filtered_pixels = reshape(filtered_frame, filtered_size(1)*filtered_size(2),
filtered_size(3));
filtered = reshape(filtered_pixels, filtered_size);
fil_unfil_pixels = filtered_pixels - unfiltered_pixels; %filtered - unfiltered ->what we
want
%This takes a pixel-by-pixel subtraction (filtered-unfiltered) to show what
%the filter did to the image.
fil_unfil = reshape(fil_unfil_pixels, unfiltered_size);
%% Now we need to convert the colors to ranges
% Red
phi_620 = 0.00689;   %(m-1) temperature and salinity corrected absorption
%coefficient for 620 nm at 27.6 C in .77 g/L salt water
Red_Shift = log(filtered_pixels./unfiltered_pixels)/(-phi_620);
min_Red = min(Red_Shift(isfinite(Red_Shift))); max_Red =
max(Red_Shift(isfinite(Red_Shift)));
for i = 1:length(Red_Shift(:,1))
   if Red_Shift(i,1) == inf
      Red_Shift(i,1) = max_Red;
   elseif Red_Shift(i,1) == -inf
```

```
        Red_Shift(i,1) = min_Red;
    end
end
Red_Matrix = reshape(Red_Shift, filtered_size);
Red_3D = Red_Matrix(:,:,1); %red pixels
phi_510 = 0.00689;   %(m-1) temperature and salinity corrected absorption
%coefficient for 510 nm at 27.6 C in .77 g/L salt water
Green_Shift = log(filtered_pixels./unfiltered_pixels)/(-phi_510);
min_Green = min(Green_Shift(isfinite(Green_Shift)));
max_Green = max(Green_Shift(isfinite(Green_Shift)));
for i = 1:length(Green_Shift(:,2))
    if Green_Shift(i,2) == inf
        Green_Shift(i,2) = max_Green;
    elseif Green_Shift(i,2) == -inf
        Green_Shift(i,2) = min_Green;
    end
end
Green_Matrix = reshape(Green_Shift, filtered_size);
Green_3D = Green_Matrix(:,:,2); %green pixels
% Blue
phi_440 = 0.00331;   %(m-1) temperature and salinity corrected absorption
%coefficient for 440 nm at 27.6 C in .77 g/L salt water
Blue_Shift = log(filtered_pixels./unfiltered_pixels)/(-phi_440);
min_Blue = min(Blue_Shift(isfinite(Blue_Shift)));
max_Blue = max(Blue_Shift(isfinite(Blue_Shift)));
for i = 1:length(Blue_Shift(:,3))
    if Blue_Shift(i,3) == inf
        Blue_Shift(i,3) = max_Blue;
    elseif Blue_Shift(i,3) == -inf
        Blue_Shift(i,3) = min_Blue;
    end
end
Blue_Matrix = reshape(Blue_Shift, filtered_size);
Blue_3D = Blue_Matrix(:,:,3); %blue pixels
% RGB is the summation of Red + Green + Blue values
RGB_3D(:,:,1) = (Red_3D + Green_3D + Blue_3D);
%% Plot results
figure(1)      %original unfiltered image
imshow(uint8(unfiltered));
figure(2)      %original filtered image
imshow(uint8(filtered));
figure(3)      %This shows the effect of the filter
imshow(uint8(fil_unfil));
figure(4)      %3D image based on red color shift, straight on view
mframe = fliplr(Red_3D);
```

```
mesh(mframe(:,:,1),'LineWidth',.3)
shading interp
axis([0,length(Red_3D(1,:)),0,length(Red_3D(:,1)),min_Red,max_Red])
xlabel('x (pixel)'); ylabel('y (pixel)'); zlabel('z (mm)')
view(180,90); colorbar;
shortname = strsplit(unf_img,'.');
shortname(1,2)= {'Red1.jpg'};
newname = strjoin(shortname);
saveas(gcf,newname,'jpg')
figure(5)      %3D image based on red color shift, rotated view
mframe = fliplr(Red_3D);
mesh(mframe(:,:,1),'LineWidth',.3)
shading interp
axis([0,length(Red_3D(1,:)),0,length(Red_3D(:,1)),min_Red,max_Red])
xlabel('x (pixel)'); ylabel('y (pixel)'); zlabel('z (mm)')
view(150,70); colorbar;
shortname(1,2)= {'Red2.jpg'};
newname = strjoin(shortname);
saveas(gcf,newname,'jpg')
figure(6)      %3D image based on green color shift, rotated view
mframe = fliplr(Green_3D);
mesh(mframe(:,:,1),'LineWidth',.3)
shading interp
axis([0,length(Green_3D(1,:)),0,length(Green_3D(:,1)),min_Green,max_Green])
xlabel('x (pixel)'); ylabel('y (pixel)'); zlabel('z (mm)')
view(150,70); colorbar;
shortname(1,2)= {'Green.jpg'};
newname = strjoin(shortname);
saveas(gcf,newname,'jpg')
figure(7)      %3D image based on blue color shift, rotated view
mframe = fliplr(Blue_3D);
mesh(mframe(:,:,1),'LineWidth',.3)
shading interp
axis([0,length(Blue_3D(1,:)),0,length(Blue_3D(:,1)),min_Blue,max_Blue])
xlabel('x (pixel)'); ylabel('y (pixel)'); zlabel('z (mm)')
view(150,70); colorbar;
shortname(1,2)= {'Blue.jpg'};
newname = strjoin(shortname);
saveas(gcf,newname,'jpg')
figure(8)      %3D image based on red + green + blue color shift, rotated view
mframe = fliplr(RGB_3D);
mesh(mframe(:,:,1),'LineWidth',.3)
shading interp
axis([0,length(RGB_3D(1,:)),0,length(RGB_3D(:,1)),min_Red,max_Blue])
xlabel('x (pixel)'); ylabel('y (pixel)'); zlabel('z (mm)')
```

```
view(150,70); colorbar;
shortname(1,2)= {'RGB.jpg'};
newname = strjoin(shortname);
saveas(gcf,newname,'jpg')
```

LIST OF REFERENCES

[1] The United States Navy. (2004, Nov.) The Navy unmanned undersea vehicle (UUV) master plan. U.S. Navy. [Online]. Available: www.navy.mil/navydata/technology/uuvmp.pdf. Accessed 25-April-2017.

[2] R. W. Button, J. Kamp, T. B. Curtain, and J. Dryden, *A Survey of Missions for Unmanned Undersea Vehicles*. Santa Monica, CA: RAND Corporation, 2009.

[3] Review of ONR's Uninhabited Combat Air Vehicles Program, Office of Naval Research, Washington, D.C., 2000, pp. 1-46.

[4] OUSD(ATL)/PSA/LW&M, "DOD unmanned systems integrated roadmap," presented at the AUVSI Unmanned Systems Program Review, Washington, DC, 2008.

[5] A.O. Hill. (2016, Jul. 07). Robot vision vs computer vision, what's the difference? [Online]. Available: http://blog.robotiq.com/robot-vision-vs-computer-vision-whats-the-difference

[6] C. Cain and A. Leonessa, "Laser based rangefinder for underwater applications," in *Proceedings of the American Control Conference*, Montreal, Canada, 2012, pp. 6190–6195.

[7] N. Hansen, M. Nielsen, D. Christensen, and M. Blanke, "Short-range sensor for underwater robot navigation using line-lasers and vision," presented at 10th IFAC Conference on Maneuvering Control of Marine Craft, Kgs. Lyngby, Denmark, 2015.

[8] G. C. Karras and K. J. Kyriakopoulos, "Localization of an underwater vehicle using an IMU and a laser-based vision system," in *IEEE Proceedings 15th Mediterranean Conference on Control & Automation*, Athens, Greece, 2007, pp. 1–6.

[9] J. S. Jaffe, "Development of a laser line scan LiDAR imaging system for AUV use," Scripps Institution of Oceanography, La Jolla, CA, Final Report, 2010.

[10] M. M. Campos and G. O. Codina, "Evaluation of a laser based structured light system for 3D reconstruction of underwater environments," in *5th MARTECH International Workshop on Marine Technology*, Girona, Spain, 2013, pp. 43–46.

[11] P. Payeur and D. Desjardins, "Dense stereo range sensing with marching pseudorandom patterns," in *Fourth Canadian Conference on Computer and Robot Vision*, Montreal, Canada, 2007, pp. 216–226.

[12] S. Fernandez, J. Salvi, and T. Pribanic, “Absolute phase mapping for one-shot dense pattern projection,” presented at the IEEE Computer Society Conference on Computer Vision and Pattern Recognition Workshops, San Francisco, CA, 2010.

[13] G. E. Dawson, “Toward a compact underwater structured light 3D imaging system,” B.S. thesis, Dept. of Mech. Eng., Massachusetts Institute of Technology, Boston, MA, 2013.

[14] A. Sarafraz and B. Haus. (2016). A structured light method for underwater surface reconstruction. *ISPRS J. Photogramm. Remote Sens*, *114*, pp. 40–52. [Online]. doi: 10.1016/j.isprsjprs.2016.01.014

[15] I. Ishii, K. Yamamoto, K. Doi, and T. Tsuji, “High-speed 3D image acquisition using coded structured light projection,” in *IEEE RSJ International Conference on Intelligent Robotics and Systems*, San Diego, CA, 2007, pp. 925–930.

[16] P. S. Huang and S. Zhang. (2006). Fast three-step phase-shifting algorithm. *Appl. Opt*, *45*, pp. 5086–5091. [Online]. doi: 10.1364/AO.45.005086

[17] F. Bruno, G. Bianco, M. Muzzupappa, S. Barone, and A. Razionale. (2011). Experimentation of structured light and stereo vision for underwater 3D reconstruction. *ISPRS J. Photogramm. Remote Sens*, *66*(4), pp. 508–515. [Online]. doi: 10.1016/j.isprsjprs.2011.02.009

[18] Visual odometry. (n.d.). Wikipedia. [Online]. Available: https://en.wikipedia.org/wiki/Visual_odometry. Accessed on 12-Apr-2017.

[19] J. Campbell, R. Sukthankar, I. Nourbakhsh, and A. Pahwa, “A robust visual odometry and precipice detection system using consumer-grade monocular vision,” presented at the IEEE International Conference on Robotics and Automation, Barcelona, Spain, 2005.

[20] M. Irani, B. Rousso, and S. Peleg, “Recovery of ego-motion using image stabilization,” presented at 1994 IEEE Computer Society Conference on Computer Vision and Pattern Recognition, Seattle, WA, 1994.

[21] W. Burger and B. Bhanu. (1990, Nov.). Estimating 3-D egomotion from perspective image sequences. *IEEE Trans. Pattern Anal. Mach. Intell*, *12*(11). [Online]. Available: http://ieeexplore.ieee.org/document/61704/

[22] A. Jaegle, S. Phillips, and K. Daniilidis, “Fast, robust, continuous monocular egomotion computation,” presented at IEEE International Conference on Robotics and Automation, Stockholm, Sweden, 2016.

[23] S. S. C. Botelho, P. Drews Jr, G. L. Olivereira, and M. S. Figueiredo, “Visual odometry and mapping for underwater autonomous vehicles,” in *6th Latin American Robotics Symposium*, Valparaiso, Chile, 2009, pp. 1–6.

[24] O. Shakernia, R. Vidal, and S. Sastry, “Omnidirectional egomotion estimation from back-projection flow,” in *IEEE Conference on Computer Vision and Pattern Recognition*, Madison, WI, 2003, vol. 7, p. 82.

[25] J. T. O. Kirk, *Light and Photosynthesis in Aquatic Ecosystems*, Cambridge, UK: Cambridge University Press, 1994.

[26] J. Adolfson and T. Berghage, *Perception and performance underwater*, Oxford, England: John Wiley and sons, 1974.

[27] Ocean explorer. (2010, Aug. 26). N.O.A.A. Office of Ocean Exploration and Research. [Online]. Available: http://oceanexplorer.noaa.gov/explorations/04deepscope/background/deeplight/media/diagram3.html.

[28] R. Garcia, T. Niscosevici, and X. Cufi, “On the way to solve lighting problems in underwater imaging,” in *IEEE Proceedings OCEANS 2002*, Biloxi, MS, 2002, pp. 1018–1024.

[29] I. Vasilescu, C. Detweiler, and D. Rus. (2011). Color-accurate underwater imaging using perceptual adaptive illumination. *Autonomous Robots*. [Online]. pp. 285–296. doi: 10.1007/s10514-011-9245-0

[30] J. Becquerel and J. Rossignol, *International Critical Tables*, vol. 5, p. 268, 1929.

[31] C. K. N. Patel and A. C. Tam. (1979, Jul.). Optical absorption coefficients of water. *Nature*, *280*, pp. 302–30.. [Online]. Available: https://www.nature.com/nature/journal/v280/n5720/abs/280302a0.html

[32] R. M. Pope and E. S. Fry. (1997). Absorption spectrum (380-700nm) of pure water. Integrating cavity measurements. *Appl. Opt*, *36*(33), pp. 8710–872. [Online]. doi: 10.1364/AO.36.008710

[33] CIE. (1932). *Commission Internationale de l’Eclairage Proceedings, 1931*. Cambridge, UK: Cambridge University Press.

[34] L. A. Jones. (1943). The historical background and evolution of the colorimetry report. *J. Opt. Soc. Am*, *33*(10), pp. 534–5.. [Online]. doi: 10.1364/JOSA.33.000534

[35] T. Smith and J. Guild. (1931). The C.I.E. colorimetric standards and their use. *Trans. Opt. Soc*, *33*(3), p. 7.. [Online]. Available: http://iopscience.iop.org/article/10.1088/1475-4878/33/3/301/meta

[36] Adobe, *Adobe RGB (1998) Color Image Encoding*, 5th ed. San Jose, CA: Adobe Systems Incorporated, 2005.

[37] Luminous intensity. (1998, Jul.20). Encyclopaedia Brittanica inc. [Online]. Available: https://www.britannica.com/science/luminous-intensity

[38] Luminous intensity. (n.d.). Wikipedia. [Online]. Available: https://en.wikipedia.org/wiki/Luminous_intensity. Accessed on 10-Apr-2017.

[39] J. H. Morrow, T. P. Comer, R. N. Lind, J. Robertson, and C. R. Booth. (2003, Jun.). A submersible radiometer for measuring solar UV irradiance over a wide dynamic range. *Proc. SPIE Ultraviolet ground- and space-based Measurements, Models, and Effects II, 4896.* [Online]. Available: http://proceedings .spiedigitallibrary.org/proceeding.aspx?articleid=881999

[40] W. S. Pegau, D. Gray, J. Ronald, and V. Zaneveld. (1997). Absorption and attenuation of visible and near-infrared light in water: dependence on temperature and salinity. *Appl. Opt*, *36*(24), pp. 6035–6046. [Online]. doi: 10.1364/AO.36.006035

[41] R. Rottgers, D. McKee, and C. Utschig. (2014, Oct.). Temperature and salinity correction coefficients for light absorption by water in the visible to infrared spectral region. *Opt. Express*, *22*(21), pp. 25093–25108. [Online]. Available: https://www.osapublishing.org/abstract.cfm?uri=oe-22-21-25093

[42] B. K. Pierson, V. M. Sands, and J. L. Frederick. (1990). Spectral irradiance and distribution of pigments in a highly layered marine microbial mat. *Appl. Environ. Microbio,* 56. pp. 2327–2340. [Online]. Available: http://aem.asm.org/ content/56/8/2327.short

[43] M. Stomp, J. Huisman, L. J. Stal, and H. C. P. Matthijs. (2007, Jul.). Colorful niches of phototrophic microorganisms shaped by vibrations of the water molecule. *ISME J, 1*, pp. 271–282 [Online]. Available: http://www.nature.com/ ismej/journal/v1/n4/full/ismej200759a.html

[44] G. Sabehi, B. C. Kirkup, M. Rozenberg, N. Stambler, M. F. Polz, and O. Beja. (2007). Adaptation and spectral tuning in divergent marine proteorhodopsins from the eastern Mediterranean and the Sargasso Seas, *ISME J, 1*, pp. 48–55. [Online]. Available: https://www.ncbi.nlm.nih.gov/pubmed/18043613

[45] Z. P. Lee, K. L. Carder, C. D. Mobley, R. G. Steward, and J. S. Patch. (1999). Hyperspectral remote sensing for shallow water. *Appl. Opt*, 38(18). pp. 3831–3843. [Online]. doi: 10.1364/AO.38.003831

[46] C. D. Mobley, H. Zhang, and K. J. Voss. (2003). Effects of optically shallow bottoms on upwelling radiances: bidirectional reflectance distribution function effects. *Limnol. Oceanogr, 48*(1), pp. 337–345. [Online]. doi: 10.4319/ lo.2003.48.1_part_2.0337/abstract

[47] D. C. English and K. L. Carder. (2006, Feb.). Determining bottom reflectance and water optical properties using unmanned underwater vehicles under clear or cloudy skies. *J. Atmospheric Ocean. Technol.* [Online]. doi: 10.1175/JTECH1842.1

[48] Standard loggers. (n.d.). RBR. [Online]. Available: https://rbr-global.com/products/standard-loggers. Accessed 20-Apr-2017.

[49] T. W. Cronin and N. Shashar. (2001). The linearly polarized light field in clear, tropical marine waters: spatial and temporal variation of light intensity, degree of polarization and e-vector angle. *J. Exp. Biol*, *204*, pp. 2461–2467. [Online]. Available: https://www.sciencebase.gov/catalog/item/50577c6ae4b01ad7e027e61b

THIS PAGE INTENTIONALLY LEFT BLANK

INITIAL DISTRIBUTION LIST

1. Defense Technical Information Center
   Ft. Belvoir, Virginia

2. Dudley Knox Library
   Naval Postgraduate School
   Monterey, California